

Glucose-sensitive insulin with attenuation of hypoglycaemia

<https://doi.org/10.1038/s41586-024-08042-3>

Received: 1 May 2023

Accepted: 12 September 2024

Published online: 16 October 2024

Open access

 Check for updates

Thomas Hoeg-Jensen¹, Thomas Kruse¹, Christian L. Brand², Jeppe Sturis², Christian Fledelius², Peter K. Nielsen¹, Erica Nishimura², Alice R. Madsen¹, Lennart Lykke¹, Kim S. Halskov¹, Simona Koščová³, Vladislav Kotek³, Anthony P. Davis⁴, Robert A. Tromans⁵, Michael Tomsett⁵, Guillem Peñuelas-Haro⁵, Daniel J. Leonard⁵, Michael G. Orchard⁵, Andy Chapman⁵, Gaetano Invernizzi¹, Eva Johansson¹, Daniele Granata⁶, Bo F. Hansen², Thomas A. Pedersen², Jonas Kildegaard², Karen-Margrethe Pedersen², Hanne H. F. Refsgaard², Lene Alifrangis², Johannes J. Fels¹, Anita V. Neutzsky-Wulff¹, Per Sauerberg² & Rita Slaaby²✉

The risk of inducing hypoglycaemia (low blood glucose) constitutes the main challenge associated with insulin therapy for diabetes^{1,2}. Insulin doses must be adjusted to ensure that blood glucose values are within the normal range, but matching insulin doses to fluctuating glucose levels is difficult because even a slightly higher insulin dose than needed can lead to a hypoglycaemic incidence, which can be anything from uncomfortable to life-threatening. It has therefore been a long-standing goal to engineer a glucose-sensitive insulin that can auto-adjust its bioactivity in a reversible manner according to ambient glucose levels to ultimately achieve better glycaemic control while lowering the risk of hypoglycaemia³. Here we report the design and properties of NNC2215, an insulin conjugate with bioactivity that is reversibly responsive to a glucose range relevant for diabetes, as demonstrated *in vitro* and *in vivo*. NNC2215 was engineered by conjugating a glucose-binding macrocycle⁴ and a glucoside to insulin, thereby introducing a switch that can open and close in response to glucose and thereby equilibrate insulin between active and less-active conformations. The insulin receptor affinity for NNC2215 increased 3.2-fold when the glucose concentration was increased from 3 to 20 mM. In animal studies, the glucose-sensitive bioactivity of NNC2215 was demonstrated to lead to protection against hypoglycaemia while partially covering glucose excursions.

Using insulin to control diabetes comes with the risk of introducing hypoglycaemia, namely blood glucose values below 3.9 mM (refs. 1,2). This is due to the fact that blood glucose fluctuations are difficult to predict owing to many factors, such as the character and timing of meals, exercise, infections and changing individual insulin sensitivity. People with diabetes must therefore adjust their daily doses of insulin (both basal and meal insulin) to account for these factors. However, to avoid events of low blood glucose, which can be dangerous especially during the night, many opt for conservative insulin doses. Compromising insulin doses due to the fear of hypoglycaemia subsequently results in suboptimal glucose control, thereby increasing the risk of complications arising from long-term hyperglycaemia. To facilitate improved glycaemic control without the risk of hypoglycaemia, the idea of engineering an insulin that can modify its bioactivity in response to varying blood glucose levels has been pursued since the 1970s³. Despite many publications and patents, to date, no mechanism has proven to solve the issue to the extent that it can be applied to treat diabetes^{5–11}. Most papers in the field describe polymer systems that can release insulin from subcutaneous (s.c.) depots in response to glucose

fluctuations, but such systems are limited by delayed glucose diffusion to the subcutis, as well as a delay in the released insulin entering the blood circulation. Moreover, such systems release insulin irreversibly, meaning that, once the insulin is released from the depot, it is no longer glucose sensitive. A better approach seems to be equipping insulin itself with glucose-responsive properties, so it can respond to glucose in a reversible manner. Notably, glucose values vary over a narrow range (from approximately 2 to 20–30 mM in people with diabetes), so a rather steep change in insulin bioactivity must be attained for the glucose-sensitive insulin to have an impact. To achieve such sensitivity to glucose, a chemical group able to bind to glucose with maximal sensitivity in this glucose range will be required. One system was based on oligofucose/mannose insulin conjugates that can be cleared from the circulation in an equilibrium between glucose-sensitive binding to the mannose receptor versus insulin binding to the insulin receptor¹², but this did not merit pursuing beyond phase I clinical trials¹³. The glucose response was found to be shallow, and high clearance at the mannose receptor led to a very low *in vivo* potency, implicating the eventual need for prohibitively high insulin doses.

¹Global Research Technologies, Novo Nordisk, Bagsværd, Denmark. ²Global Drug Discovery, Novo Nordisk, Bagsværd, Denmark. ³APIGENEX, Prague, Czech Republic. ⁴University of Bristol, Bristol, UK. ⁵Carbometrics, Bristol, UK. ⁶Digital Science and Innovation, Novo Nordisk, Bagsværd, Denmark. ✉e-mail: risl@novonordisk.com

The concept of introducing a glucose-sensitive switch into the insulin molecule has been pursued over many years^{1,14–16}. A switch involves dual conjugation of a glucose-binding motif plus a binding partner onto insulin such that, at low glucose, the switch will induce a closed less-active state, equilibrating towards an open more-active state with higher glucose concentrations. The glucose-binding motif must therefore have an affinity for both glucose and the binding partner within the narrow glucose range that occurs in people with diabetes (approximately 2 to 20–30 mM). Furthermore, the two components of the switch must be attached to insulin in a manner that ensures that, in the closed state, there is a lower insulin bioactivity by altering the insulin conformation and/or blocking the receptor binding surfaces of insulin. This switch idea has been pursued by using boronates as glucose binders, but the glucose sensitivity of such designs has so far been too limited for pharmacological use. The best previous example of a carbohydrate-sensitive switch working with insulin showed sensitivity to fructose at high concentrations (50 mM), but the compound was insensitive to glucose¹⁵. A recently identified macrocycle offers another option for a glucose-binding element⁴. The macrocycle was designed to provide a glucose-binding cavity that secures a relevant affinity for glucose as well as selectivity over other carbohydrates and potentially interfering small molecules. Here we describe the molecular design of NNC2215, an insulin with a glucose switch by incorporating the macrocycle at B29Lys and introducing an *O*1-glucoside through a short linker at B1Phe (Fig. 1a). This combination of glucose binder, glucoside, linker and conjugation sites was found to impart glucose-sensitive bioactivity to NNC2215, which demonstrated a 12.5-fold increase in insulin receptor binding affinity when glucose was raised from 0 to 20 mM and a 3.2-fold increase when raised from 3 to 20 mM. Furthermore, NNC2215 was shown to be glucose sensitive *in vivo*, to attenuate hypoglycaemia in pigs and to reduce the glucose excursions during glucose tolerance tests (GTTs) in diabetic rats.

Chemistry

The macrocycle⁴ (Fig. 2a) was conjugated to desB30 human insulin at the B29Lys *N*⁶ amino group through triazole formation¹⁷ between a macrocycle derivative carrying an azido propyl linker from the macrocycle roof and an alkyne linker attached to B29Lys (by conjugation at pH > 10 to obtain the B29 product). Conjugation through the macrocycle roof circumvents the need to orthogonally address one of three carboxylic acids, as would be needed for conjugation to either of the COOH groups on the pillars of the macrocycle. Dendrimers that were used for securing good aqueous solubility of the originally reported macrocycle⁴ were found to be unnecessary when working with insulin–macrocycle conjugates. Besides the macrocycle at B29, an *O*1-glucoside with a short linker was attached to the B-chain N-terminal amino group (PheB1) by using the corresponding bromo trifluoromethyl sulfate phenyl ester at pH 7.5 (ref. 18). The glucoside was used as its *O*-peracetyl protected building block, and the acetyl groups were removed from the insulin conjugate by gentle saponification. A control compound, NNC2215a, with only the macrocycle at B29 was prepared similarly to NNC2215 by omitting the glucoside step. The conjugation sites on insulin were documented by liquid chromatography coupled with mass spectrometry (LC–MS) analysis of a sample that was treated with trypsin followed by tris(2-carboxyethyl)phosphine (TCEP). The trypsin treatment cleaved NNC2215 after B22Arg to release the B23–B29 fragment, and TCEP cleaved the disulfides of NNC2215 to give separate A and B chains. LC–MS analysis of the resulting analytical mixture showed the macrocycle attached to the B23–B29 fragment, and the glucoside attached to the B1–B22 fragment, along with free A-chain (chemistry details and LC–MS spectra are provided in the Supplementary information and Supplementary Data).

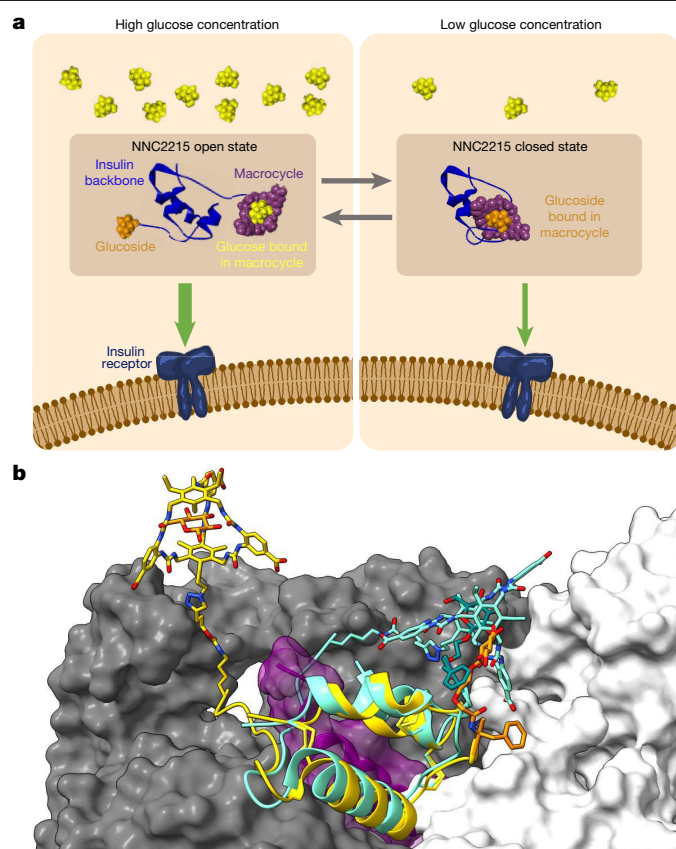


Fig. 1 | Functional principle and 3D model of NNC2215. **a**, NNC2215 is an insulin molecule with a glucose-sensitive switch. At increasing glucose concentrations, the switch equilibrates towards an open state and the insulin receptor affinity of NNC2215 is high, thereby contributing to preventing hyperglycaemia. When glucose levels decrease, the switch equilibrates towards a closed state, interfering with the ability of NNC2215 to bind to the insulin receptor, thereby contributing to preventing hypoglycaemia. Insulin backbone, macrocycle, glucoside and glucose models were prepared using BIOVIA Discovery Studio (Dassault Systèmes). **b**, 3D models of NNC2215 in the open and closed forms. The insulin backbone is shown as ribbons and the switch elements (glucoside and macrocycle) are shown as stick representations. Insulin receptor chains A and C from PDB 6PXV are shown as white and grey surface representations. The open form of NNC2215 (yellow) has free glucose (orange; top left corner) bound to the macrocycle at B29. The B1–glucoside of NNC2215 in the open form is shown in orange (on the right). The closed form of NNC2215 (cyan) has the glucoside bound in the macrocycle and shows a clash between the C-terminal part of the insulin B-chain, including the switch and the C-terminal domain of the insulin receptor (α -CT, purple).

Glucose binding of macrocycle and NNC2215

Using isothermal titration calorimetry (ITC), the free macrocycle of NNC2215 was shown to bind to glucose with a dissociation constant (K_d) of 98 μ M (Fig. 2b). Native MS analysis was used to study the binding of NNC2215 towards glucose. As expected, the presence of the glucoside in the dual conjugate changed the glucose affinity of NNC2215 relative to the free macrocycle, such that NNC2215 was found to bind to glucose with a K_d of 2.1 mM, which, in the context of diabetes, is considered to be severe hypoglycaemia. The control compound, NNC2215a with macrocycle only, was found by native MS to bind to glucose with a K_d of 0.5 mM. It is not surprising that conjugation of the macrocycle to insulin will moderately change its glucose affinity (relative to the free macrocycle). Similarly, attaching albumin-binding moieties to insulin or other proteins also generally changes their affinity relative to the free ligands, probably due to weak interactions of the conjugated moieties

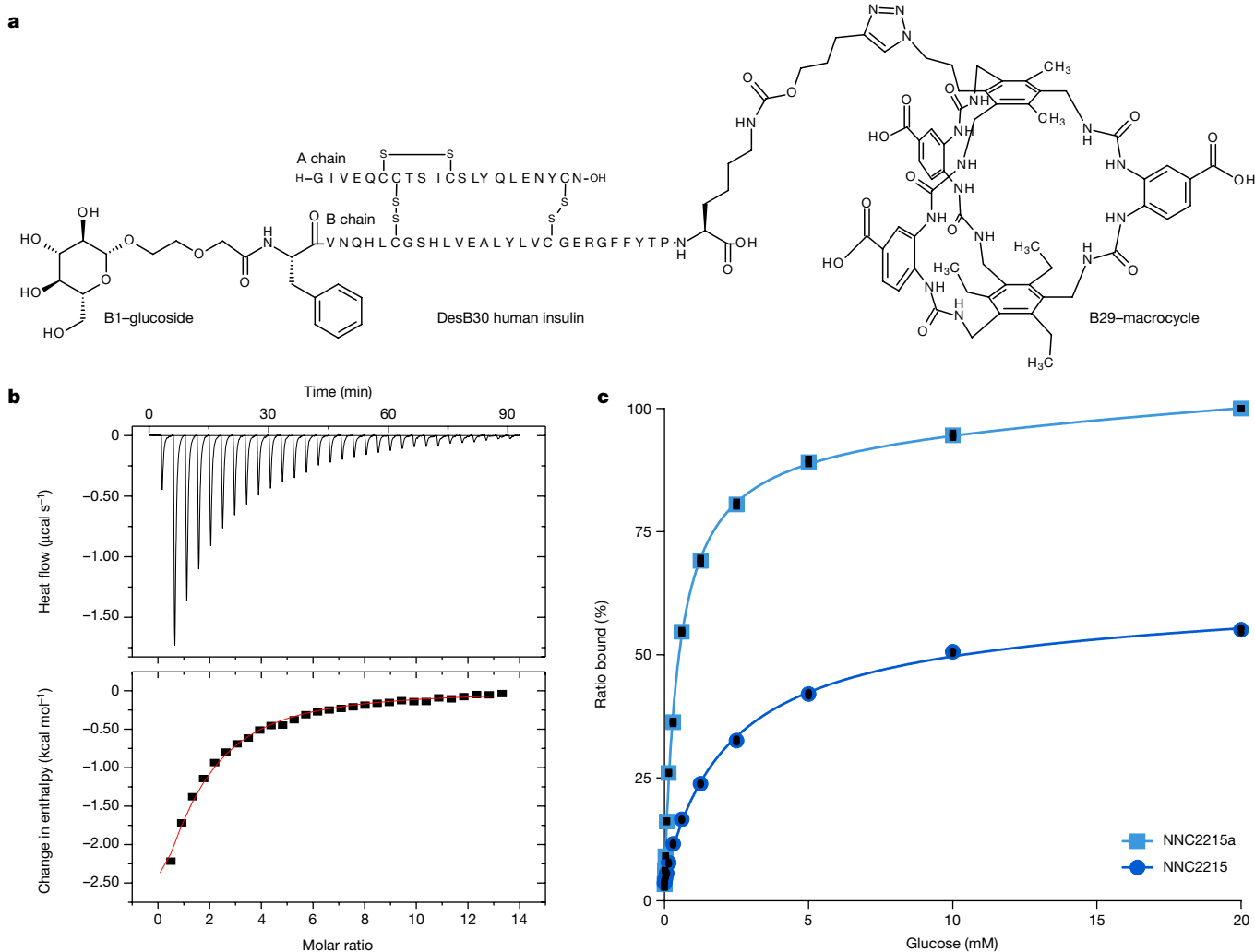


Fig. 2 | Chemical structure and glucose-binding properties of NNC2215.

a, NNC2215 with dual conjugation of the macrocycle at B29 and the glucoside at B1. The control compound NNC2215a has only the B29-macrocycle. Prepared using BIOVIA Draw (Dassault Systèmes). **b**, ITC measurement of the affinity of glucose to the free macrocycle. A K_d of 98 μM was obtained by fitting the data to a 1:1 binding model. **c**, Analysis of the binding of glucose towards NNC2215

with the proximal protein and its sidechains. Overall, the glucose affinity of NNC2215 and the control compound NNC2215a as measured by native MS was approximately 20-fold and 5-fold weaker compared with the free macrocycle, thereby demonstrating that suitable switch dynamics had been achieved. The glucose binding and concurrent opening of the switch in NNC2215 and NNC2215a in response to 0 to 20 mM glucose can be followed by the native MS binding plot in Fig. 2c. The steepest part of the binding curve is consistent with what would be considered to be hypoglycaemia, below 4 mM glucose. Although the native MS data are obtained in the gas phase (MS vacuum), such data often reflect the interactions of molecules corresponding to the aqueous solutions from which the complexes are sampled¹⁹.

3D model of NNC2215–insulin receptor

Structural models were built of the insulin receptor binding to NNC2215 with the switch in either the open or closed state by superimposing models of NNC2215 on the insulin–insulin receptor complex Protein Data Bank (PDB) 6PXV (refs. 20–24) to exemplify its functioning. As illustrated in Fig. 1b, when the switch is closed, a clash occurs between the C-terminal part of the insulin B-chain and the C-terminal domain of

the insulin receptor, termed α -CT. The α -CT domain is known to be a crucial part for insulin binding²⁵. We believe that this steric hindrance is the driving force for the observed lower receptor affinity of NNC2215 at low glucose concentrations, that is, with the switch populating mainly the closed conformation. By contrast, the model of the open state is compatible with a fully active insulin conformation able to bind to the receptor.

In vitro biology

To study the glucose-sensitive interaction of NNC2215 with the insulin receptor in vitro, insulin-receptor-binding studies were conducted in the absence or presence of varying glucose concentrations whereby the binding of human insulin receptor A (hIR-A) to NNC2215 was compared to that of human insulin and insulin degludec (an acylated, long-acting basal insulin)²⁶ (Fig. 3a–c). Unique to NNC2215, it can be seen that the binding curves are affected by the increasing glucose concentrations (Fig. 3a). Relative to the hIR-A affinity for human insulin, the affinity for NNC2215 increases from 0.75% to 2.9%, 4.3%, 6.5% and 9.2% over the glucose concentration range of 0, 3, 5, 10 and 20 mM, whereas insulin degludec has a constant affinity relative to human insulin (Table 1

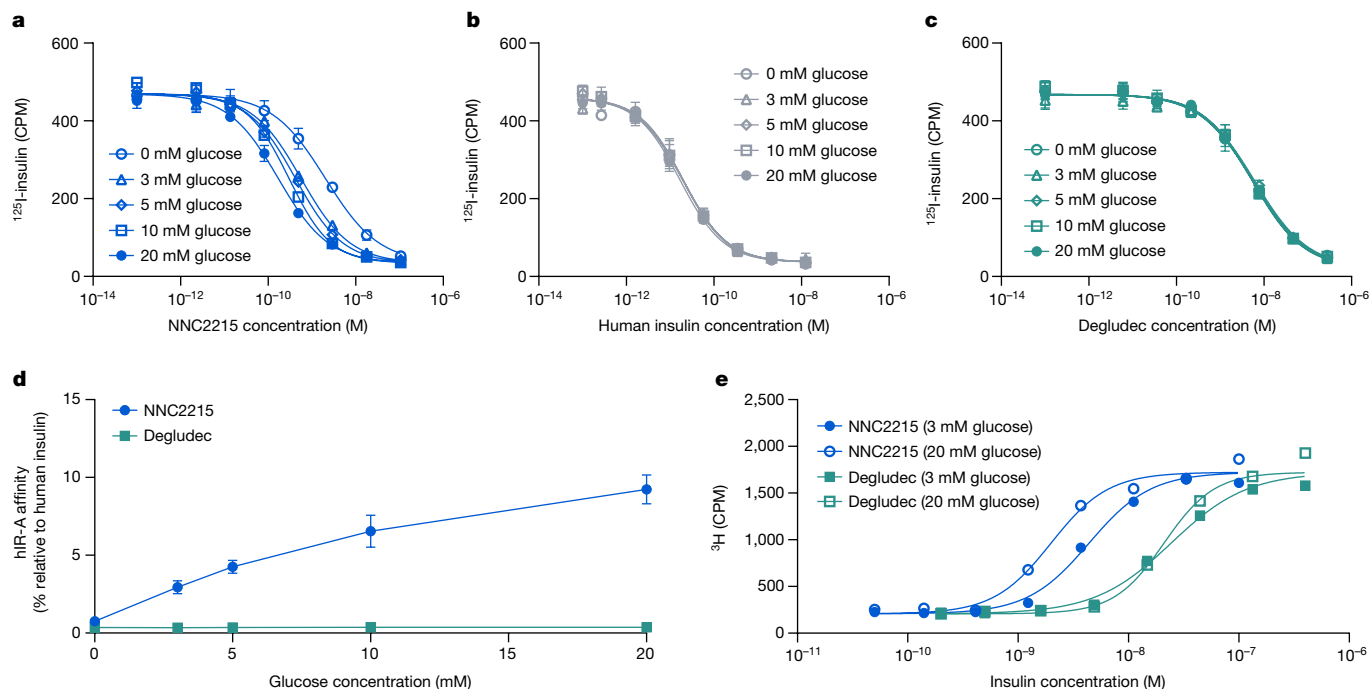


Fig. 3 | Glucose-dependent hIR-A affinity of NNC2215. **a–c**, Representative displacement curves of ¹²⁵I-insulin from hIR-A for NNC2215 (**a**), human insulin (**b**) and insulin degludec (**c**) in the presence of 0 to 20 mM D-glucose. Data are mean ± s.d. *n* = 3 technical replicates. For some datapoints, the s.d. error bars are shorter than the size of the symbols. **d**, hIR-A affinity of NNC2215 and insulin degludec relative to human insulin over increasing glucose concentrations.

Data are mean ± s.d. *n* = 3 independent replicates. For some datapoints, the s.d. error bars are shorter than the size of the symbols. **e**, Representative curves of NNC2215 and insulin degludec dose-dependent conversion of ³H-D-glucose into lipid in isolated rat adipocytes at low (3 mM) and high (20 mM) L-glucose concentrations. Data are mean. *n* = 2 technical replicates. CPM, counts per minute.

and Fig. 3d). The increase in hIR-A affinity for NNC2215 is 12.5-fold from 0 to 20 mM glucose, while it is 3.2-fold from 3 to 20 mM glucose, a concentration range that can be observed in people with diabetes (Table 1). Notably, this increase in hIR-A affinity was determined in the presence of 1.5% albumin, which is the maximum concentration that can be tolerated in the assay (compared to approximately 4% albumin in the human circulation). In the absence of albumin, the increase in hIR-A affinity was reduced to 6.8-fold (from 0 to 20 mM glucose), suggesting that albumin binding contributes to some extent to the glucose sensitivity of NNC2215 (Extended Data Fig. 1a). Furthermore, the observation that, in the presence of 1.5% albumin, there is a small, 2.4-fold increase in hIR-A affinity (from 0 to 20 mM glucose) for NNC2215a, the control compound with only a macrocycle, also indicates a weak albumin-binding effect (Extended Data Fig. 1b).

The specificity towards the insulin receptor compared to the insulin-like growth factor 1 receptor (IGF-1R) is very important to avoid any increased mitogenicity. The IGF-1R binding was measured in the presence and absence of 20 mM D-glucose (Extended Data Fig. 1c). Relative to human insulin, at both 0 and 20 mM glucose, NNC2215 had approximately 10% IGF-1R affinity compared with its insulin receptor affinity (Extended Data Fig. 1a,d). Thus, as compared to human insulin, NNC2215 has a higher specificity towards the insulin receptor versus the IGF-1R.

The ability of NNC2215 to activate the insulin signalling pathway was examined in Chinese hamster ovary cells expressing the cloned human insulin receptor (CHO-hIR). Full dose–response curves were obtained for NNC2215 stimulating tyrosine phosphorylation of the human insulin receptor with a potency of 57.1% (95% confidence interval

Table 1 | Glucose sensitivity of NNC2215 activity with respect to hIR-A binding and downstream metabolic response

	hIR-A affinity relative to human insulin ^a (%)					
	D-Glucose (mM)			L-Glucose (mM)		
	0	3	5	10	20	20
NNC2215	0.75 ± 0.1	2.9 ± 0.4	4.3 ± 0.4	6.5 ± 1.0	9.2 ± 0.9	5.7 ± 0.8
Insulin degludec	0.36 ± 0.01	0.35 ± 0.03	0.36 ± 0.03	0.37 ± 0.03	0.37 ± 0.04	0.49 ± 0.08
	hIR-A affinity relative to human insulin (fold change between glucose concentrations)			Lipogenesis (fold change between glucose concentrations)		
	D-Glucose (mM)		L-Glucose (mM)			
	20 vs 3	20 vs 0	20 vs 0	20 vs 3		
NNC2215	3.2 ± 0.3	12.5 ± 1.7	7.6 ± 0.8	2.2 ± 0.5		
Insulin degludec	1.1 ± 0.2	1.0 ± 0.1	1.4 ± 0.2	1.1 ± 0.2		

Data on hIR affinity are mean ± s.d. of three independent experiments. Data on lipogenesis are mean ± s.d. of seven independent experiments for NNC2215 and five independent experiments for insulin degludec.

^aDetermined from the half-maximal inhibitory concentration (IC₅₀) in the presence of 0, 3, 5, 10 or 20 mM D-glucose or 20 mM L-glucose (with 1.5% human serum albumin).

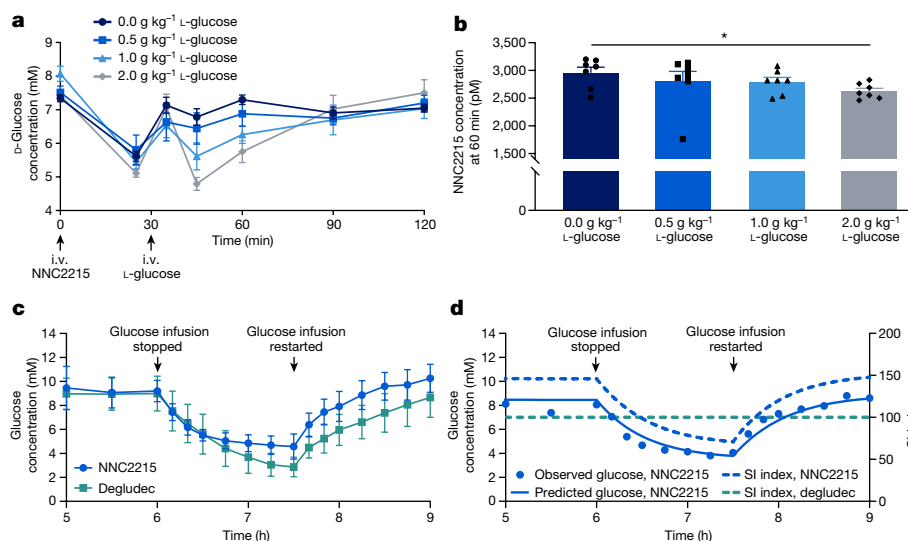


Fig. 4 | Glucose-concentration-sensitive activation and deactivation of NNC2215 in vivo. **a**, Triggering of NNC2215 by dosing rats i.v. with 0 to 2 g kg⁻¹ L-glucose, resulting in lowering of D-glucose. Data are mean ± s.e.m. *n* = 7 animals per group. **b**, Glucose dose-dependent clearance of NNC2215 measured by the NNC2215 concentration at 60 min. Data are mean ± s.e.m. *n* = 7 animals per group. Statistical analysis was performed using a two-sided Student's *t*-test;

P* = 0.013. **c, Representative glucose profiles in LYD pigs during constant i.v. infusion of NNC2215 (1.86 pmol kg⁻¹ min⁻¹) or insulin degludec (0.9 pmol kg⁻¹ min⁻¹) after stopping and restarting the constant i.v. glucose infusion (6 mg kg⁻¹ min⁻¹). Data are mean ± s.d. *n* = 7 (NNC2215) and *n* = 8 (insulin degludec) pigs. **d**, Pharmacokinetic/pharmacodynamic modelling results for a representative LYD pig dosed with 1.72 pmol kg⁻¹ min⁻¹ NNC2215. SI, insulin sensitivity index.

(CI) = 41.7–78.1) compared with human insulin. Downstream signalling through AKT and ERK activation had the same balance relative to human insulin with potencies of 68.4% (95% CI = 55.7–84.0) and 48.0% (95% CI = 34.4–66.9), respectively (Extended Data Fig. 1e–g).

The glucose sensitivity of NNC2215 was reflected in a metabolic end point measured ex vivo in rat adipocytes²⁷. The induction of glucose uptake and incorporation into lipids in rat adipocytes, that is, lipogenesis, was measured in an assay in which we took advantage of the enantiomer of the physiologically active D-glucose, namely L-glucose. The rationale for using L-glucose is that cells do not catabolize or take up L-glucose in appreciable amounts, at least not through saturable transport, except in the case of some Gram-negative bacteria and plants under certain conditions²⁸. In control experiments, L-glucose did not compete with the uptake of D-glucose into adipocytes, but L-glucose binds to the achiral macrocycle of NNC2215 with the same affinity as D-glucose²⁹. In the hIR-A-binding assay, L-glucose is not as potent as D-glucose in activating NNC2215. The increase in the binding affinity of NNC2215 observed between 0 and 20 mM is 7.6-fold for L-glucose compared with 12.5-fold for D-glucose (Table 1). The metabolic response measured with L-glucose will therefore be underestimated compared with the effect of D-glucose. The lipogenesis measurement showed a 2.2-fold difference in the dose leading to half-maximal effect determined for NNC2215-induced ³H-D-glucose conversion into lipid in rat adipocytes at low (3 mM) versus high (20 mM) L-glucose (Fig. 3e). This demonstrates the glucose sensitivity of NNC2215 ex vivo with respect to insulin-induced metabolic response. With insulin degludec, lipogenesis showed no response to L-glucose.

In vivo pharmacology

To investigate the glucose-concentration-sensitive activation and deactivation of NNC2215 in vivo, we developed three different protocols. In the simplest protocol, rats were dosed intravenously with NNC2215 followed by L-glucose, thereby triggering NNC2215, resulting in the lowering of D-glucose in an L-glucose-dose-dependent manner. Furthermore, the deactivation of NNC2215 at low glucose was investigated in pigs by an acute drop in plasma glucose in comparison to the glucose drop induced by a non-glucose-sensitive insulin (insulin degludec).

Finally, the activation of NNC2215 during meal-like glucose fluctuations was studied during a glucose challenge in diabetic rats. Insulin degludec was used as a control in the intravenous (i.v.) rat study and as a comparator in the pig study due to similar pharmacokinetic properties after i.v. administration (Extended Data Table 1a), whereas human insulin was used as comparator in the rat glucose challenge study. The in vivo half-life of NNC2215 was determined to be 1.2 h by i.v. dosing to rats and 1.3 h by i.v. dosing to pigs (Extended Data Table 1a).

L-Glucose study in rats

L-glucose was used to trigger NNC2215 in rats, without triggering endogenous insulin release as dosing of D-glucose would otherwise do in non-diabetic rats. Figure 4a shows how i.v. administration of the same dose of NNC2215 followed by L-glucose (4 dose levels including vehicle) dose-dependently triggers insulin action of NNC2215 by lowering of D-glucose. As expected, NNC2215 is dose-dependently cleared from the plasma after the triggering by L-glucose, as evidenced by the lowering of NNC2215 plasma concentrations (Fig. 4b). The initial peak in D-glucose after L-glucose or vehicle injection (Fig. 4a) is a short-lived response related to the dosing (handling) of the animals. This response is not associated with NNC2215 as the same pattern is also seen in a similar L-glucose protocol testing the non-glucose-sensitive insulin degludec (Extended Data Fig. 2). Notably, the method used to measure D-glucose does not detect L-glucose, as it is based on the glucose oxidase enzyme.

Hypoglycaemic study in LYD pigs

To evaluate the in vivo activity of NNC2215 in healthy Landrace–Yorkshire–Duroc (LYD) pigs, and to essentially eliminate the effects from D-glucose fluctuations on endogenous hormone release, somatostatin infusion was used to suppress secretion of both glucagon and insulin. Furthermore, the study was conducted under a primed constant infusion of NNC2215 versus insulin degludec at different rates accompanied by glucagon replacement and constant glucose infusion. After 5 h of infusion, when approximate steady-state plasma concentrations of insulin (degludec or NNC2215) and glucose were achieved, the D-glucose infusion was stopped (Fig. 4c). This procedure resulted in a

decrease in plasma D-glucose, promoted by the continued insulin infusion, but the drop was observed to be less pronounced with NNC2215 compared with insulin degludec, thereby showing glucose-sensitive switching of the insulin bioactivity. Evaluation of the full dataset using different insulin infusion rates of NNC2215 and insulin degludec shows that, after the glucose infusion is turned off, at any given plasma glucose concentration, the drop in plasma glucose is smaller for NNC2215 than for insulin degludec (Extended Data Fig. 3). The large s.d. observed in the C-peptide response (Extended Data Fig. 3d) was due to a single animal with high C-peptide levels during all six experimental days. Omission of the data from this animal does not alter the conclusion on glucose sensitivity (Extended Data Fig. 3c). Data from two representative groups are shown in Fig. 4c, where glucose dropped to about 4.5 mM with NNC2215 versus a drop to about 3 mM glucose for insulin degludec, thus demonstrating protection against hypoglycaemia with NNC2215.

NNC2215 exposure and plasma glucose concentrations after s.c. versus i.v. administration of NNC2215 to female LYD pigs are shown in Extended Data Fig. 4. The mean \pm s.d. bioavailability of NNC2215 after s.c. administration was estimated to be $73 \pm 24\%$. A small, acute plasma-glucose-lowering effect was observed after i.v. administration of 0.3 nmol kg^{-1} , while after s.c. administration of 2 nmol kg^{-1} , the drop in plasma glucose was less, consistent with the exposure of NNC2215. A protracted pharmacokinetic profile was observed after s.c. administration with a harmonic mean half-life of 19 h. This is longer than previously observed for insulin detemir (6.5 h)³⁰ and insulin degludec (7.2 h)³¹ in pigs and suggests that NNC2215 could be suitable for once-daily dosing based on this animal model. The difference in s.c. half-life between the different insulin analogues highlights the rationale for using i.v. infusion as the route of administration in the pig studies to demonstrate in vivo glucose sensitivity of NNC2215, which was to circumvent the confounding effects of the different s.c. pharmacokinetic profiles.

Pharmacokinetic/pharmacodynamic models

The pharmacodynamic data from pigs were analysed by applying the minimal model, which describes glucose kinetics and insulin activity in a quantitative manner³² (Supplementary information and Extended Data Fig. 5a). Together with a pharmacokinetic model (Supplementary information and Extended Data Table 1b), the minimal model was used to quantify the change in insulin activity of NNC2215 with changing plasma glucose. The best fit to the glucose data for NNC2215 from the hypoglycaemic study in LYD pigs was obtained by implementing a saturable effect of glucose on the insulin sensitivity parameter (SI) and the corresponding SI index, which is defined as 100% at 5.5 mM glucose. A representative fit to the glucose data from a single pig dosed with $1.72 \text{ pmol kg}^{-1} \text{ min}^{-1}$ NNC2215 is shown in Fig. 4d. For this pig, the plasma glucose dropped from 8.5 mM to 3.8 mM when the glucose was turned off, and the SI index decreased from 140% to 70%, indicating a significant dynamic range for activation of NNC2215 within a relevant glucose range. For insulin degludec, the SI index was always 100%, as indicated by the horizontal dashed line in Fig. 4d. The modelling indicates that, within the range of 3 to 15 mM glucose, the relationship between plasma glucose and the SI index is linear, with a slope of 14.6% per mM glucose (Extended Data Fig. 5b).

Glucose tolerance in STZ-diabetic rats

Insulinopenic streptozotocin (STZ)-diabetic rats were used to investigate the glucose-induced activation of NNC2215 without interference from endogenous insulin release during an i.v. GTT. Overnight-fasted rats were infused i.v. with one of three different constant molar rates of either NNC2215 or human insulin to lower plasma glucose from $\geq 15 \text{ mM}$ to a predefined target of 5.7 mM. This glucose target was then maintained by adjusting an i.v. glucose infusion rate. When the glucose

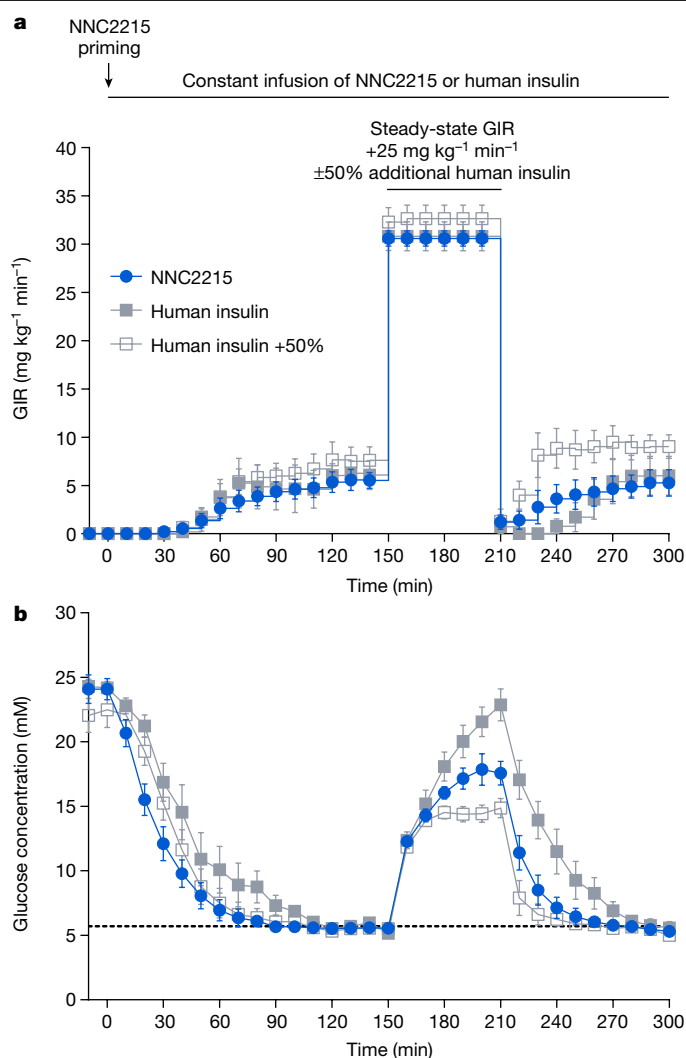


Fig. 5 | Glucose-induced activation of NNC2215 during a GTT in streptozotocin-diabetic rats. a, b, The glucose infusion rate (GIR) (a) and plasma glucose (b) profiles before (0–150 min), during (150–210 min) and after (210–300 min) a GTT in streptozotocin-diabetic rats receiving i.v. infusion of NNC2215 ($84 \text{ pmol kg}^{-1} \text{ min}^{-1}$), human insulin ($20 \text{ pmol kg}^{-1} \text{ min}^{-1}$) or human insulin ($20 \text{ pmol kg}^{-1} \text{ min}^{-1}$) plus additional $10 \text{ pmol kg}^{-1} \text{ min}^{-1}$ (+50%) during the GTT. Data are mean \pm s.e.m. $n = 5$ (NNC2215 and human insulin) and $n = 7$ (human insulin +50%) rats.

infusion rate was at steady state, a GTT was performed by infusing an additional $25 \text{ mg kg}^{-1} \text{ min}^{-1}$ of glucose for 60 min on top of the individual steady-state glucose infusion rate (Fig. 5a), and the resulting changes in the plasma glucose concentrations were then monitored.

A subset of data from STZ-diabetic rats with a similar steady-state glucose infusion rate, that is, with a similar insulin effect, before the GTT are shown in Fig. 5. As shown in Fig. 5b, during the GTT, the increase in plasma glucose was approximately 20% smaller in the NNC2215 group compared with the human insulin group (mean \pm s.e.m., 18.3 ± 1.1 versus $22.9 \pm 1.3 \text{ mM}$, $P < 0.02$), indicating a larger insulin effect of NNC2215 at the high glucose concentrations without a change in insulin exposure. To quantify how much 50% additional human insulin would reduce the maximum plasma glucose concentrations during the GTT, another group of rats was given 50% additional human insulin on top of its constant infusion rate, that is, $20 + 10 \text{ pmol kg}^{-1} \text{ min}^{-1}$ during the GTT. The resulting maximum plasma glucose concentration was significantly reduced (by approximately 34%) by the 50% additional human insulin compared to human insulin at the equimolar infusion rate (mean \pm s.e.m.

15.1 ± 0.7 versus 22.9 ± 1.3 mM, $P < 0.0002$), and the maximum plasma glucose also tended to be further reduced compared with NNC2215 (mean ± s.e.m., 15.1 ± 0.7 versus 18.3 ± 1.1 mM, $P = 0.08$) (Fig. 5b).

Analysis of the full dataset showed that, during the GTT, the reductions in the maximum plasma glucose concentration caused by NNC2215 and by the 50% additional human insulin compared to human insulin at the equimolar infusion rate were comparable across the different insulin doses tested. The glucose-induced increase in insulin activity of NNC2215 during the GTT was estimated to correspond to an approximately 30% increase in the human insulin dose (Extended Data Fig. 6).

Discussion

Insulin was equipped with a glucose-sensitive switch comprising a macrocycle conjugated to LysB29 and an O1-glucoside conjugated to B1Phe, both through short linkers. The binding of NNC2215 to glucose was evaluated using native MS analysis, showing that the steepest part of the binding curve matches the hypoglycaemic range, that is, lower than 4 mM glucose. Glucose-sensitive binding of NNC2215 to the insulin receptor over a glucose concentration range from 0 to 20 mM was measured, and the glucose responsiveness of NNC2215 was found to be much stronger than what has been reported for previous attempts at equipping insulin with glucose-sensitive switches¹. The glucose-promoted modulation of the interaction of NNC2215 with the insulin receptor could be rationalized by 3D molecular modelling studies, visualizing how NNC2215 with the switch in the closed state can interfere with binding towards the α -CT domain of the insulin receptor. To be useful as a pharmacological agent, this switch should respond to glucose in concentrations that occur in people with diabetes (that is, approximately 2 to 20–30 mM). The glucose specificity of the macrocycle has been studied previously⁴, but it cannot be ruled out that there may be some binding to glycosylated proteins. However, when looking at the insulin receptor, which is a glycosylated protein and was semi-purified using a glycosylation binding column with wheat germ agglutinin (WGA), if there was binding of NNC2215 to the glycans of the insulin receptor, the control compound NNC2215a, with only the macrocycle, should show glucose sensitivity in the binding assay, which it did not. This suggests that NNC2215 does not bind to any major extent to glycosylated proteins.

The glucose sensitivity in vivo was supported in a relatively simple, acute rat model using L-glucose dosed to trigger the insulin effect of NNC2215 without stimulating endogenous insulin release. The activation of NNC2215 by L-glucose resulted in a dose-dependent lowering of D-glucose and concurrent L-glucose dose-dependent clearance of NNC2215. This protocol was inspired by the use of α -methyl-D-mannopyranose to trigger glucose-sensitive insulin derivatives that rely on the previously described mannose receptor principle¹².

Notably, the glucose-sensitive insulin receptor binding and cellular effects of NNC2215 translated to an in vivo hypoglycaemia protective effect observed in an acute-diabetic-like pig model induced by somatostatin and glucagon replacement infusions. For the same glucose-lowering effect at the start, when the D-glucose infusion was shut off, we observed a drop in plasma glucose, but the drop was smaller for NNC2215 than for insulin degludec, with the lowest glucose value averaging approximately 4.5 mM for NNC2215 versus below 3 mM for insulin degludec. The difference in the glucose drop between NNC2215 and insulin degludec was observed across all dose levels tested and was estimated to be approximately 1.8 mM in the overlapping starting glucose range (Extended Data Fig. 3). This degree of attenuation in the undesirable plasma glucose lowering effect when there is too much insulin at low glucose levels is expected to confer a substantial advantage to insulin conjugates like NNC2215 in their ability to reduce the risk of hypoglycaemia inherent to insulin treatment whenever there is a mismatch between insulin dose and actual need.

We also observed an activation of NNC2215 during a glucose challenge in STZ-diabetic rats corresponding to the effect of 30% additional human insulin. Such glucose-induced activation of NNC2215 suggests that it may be able to contribute to reducing some of the glucose excursion after a meal. Thus, less than full doses of fast-acting insulin may be required with larger meals. Smaller doses of mealtime insulin in combination with NNC2215 could potentially reduce the risk of hypoglycaemia induced by the fast-acting insulin, and could overall allow for tighter glucose control without the fear of hypoglycaemia.

The modelling of pharmacokinetic/pharmacodynamic data in pigs quantified the dynamic range for activation of NNC2215 in vivo. On the basis of the pharmacokinetic/pharmacodynamic modelling, within the glucose range relevant for diabetes, the insulin activity index varied from around 60% at 3 mM glucose to 290% at 20 mM glucose (Extended Data Fig. 5b), that is, a 5-fold range, which matches the 3.2-fold difference in insulin receptor affinity between 3 and 20 mM glucose found in vitro. Such consistency between in vitro and in vivo glucose sensitivity of NNC2215 lends support to the possible translation to human use for compounds with properties like NNC2215.

In conclusion, insulin conjugates with properties such as NNC2215 hold promise for improving treatment of diabetes by potentially lowering the risk of hypoglycaemia and partly covering the need for fast-acting insulin at mealtime. The combination of these two features should allow for more aggressive insulin titration compared to current insulin therapies to achieve normal glucose levels without increasing the risk of hypoglycaemia. This could improve both the short-term and long-term risks and complications associated with diabetes. On a general note, NNC2215 illustrates how molecular switches can be designed to enable autonomous control of molecular bioactivity in response to changing concentrations of another molecule, even within a narrow range such as is the case for blood glucose levels.

Online content

Any methods, additional references, Nature Portfolio reporting summaries, source data, extended data, supplementary information, acknowledgements, peer review information; details of author contributions and competing interests; and statements of data and code availability are available at <https://doi.org/10.1038/s41586-024-08042-3>.

1. Hoeg-Jensen, T. Review: glucose-sensitive insulin. *Mol. Metab.* **46**, 101107 (2021).
2. ElSayed, N. A. et al. Glycemic targets: standards of care in diabetes—2023. *Diabetes Care* **46**, S97–S110 (2023).
3. Brownlee, M. & Cerami, A. A glucose-controlled insulin-delivery system: semisynthetic insulin bound to lectin. *Science* **206**, 1190–1191 (1979).
4. Tromans, R. A. et al. A biomimetic receptor for glucose. *Nat. Chem.* **11**, 52–56 (2019).
5. Veiseth, O., Tang, B. C., Whitehead, K. A., Anderson, D. G. & Langer, R. Managing diabetes with nanomedicine: challenges and opportunities. *Nat. Rev. Drug Discov.* **14**, 45–57 (2015).
6. Zaykov, A. N., Mayer, J. P. & DiMarchi, R. D. Pursuit of a perfect insulin. *Nat. Rev. Drug Discov.* **15**, 425–439 (2016).
7. Bakh, N. A. et al. Glucose-responsive insulin by molecular and physical design. *Nat. Chem.* **9**, 937–944 (2017).
8. Yu, J., Zhang, Y., Yan, J., Kahkoska, A. R. & Gu, Z. Advances in bioresponsive closed-loop drug delivery systems. *Int. J. Pharm.* **544**, 350–357 (2018).
9. VandenBerg, M. A. & Webber, M. J. Biologically inspired and chemically derived methods for glucose-responsive insulin therapy. *Adv. Healthc. Mater.* **8**, e1801466 (2019).
10. Disotuar, M. M., Chen, D., Lin, N. P. & Chou, D. H. Glucose-responsive insulin through bioconjugation approaches. *J. Diabetes Sci. Technol.* **14**, 198–203 (2020).
11. Jarosinski, M. A., Dhayalan, B., Rege, N., Chatterjee, D. & Weiss, M. A. ‘Smart’ insulin-delivery technologies and intrinsic glucose-responsive insulin analogues. *Diabetologia* **64**, 1016–1029 (2021).
12. Kaarsholm, N. C. et al. Engineering glucose responsiveness into insulin. *Diabetes* **67**, 299–308 (2018).
13. Visser, S. A. G., Kandala, B., Fancourt, C., Krug, A. W. & Cho, C. R. A model-informed drug discovery and development strategy for the novel glucose-responsive insulin MK-2640 enabled rapid decision making. *Clin. Pharmacol. Ther.* **107**, 1296–1311 (2020).
14. Zion, T. C. & Lancaster, T. M. Soluble non-depot insulin conjugates and uses thereof. Patent WO/2010/107520 (2010).
15. Chen, Y. S. et al. Insertion of a synthetic switch into insulin provides metabolite-dependent regulation of hormone-receptor activation. *Proc. Natl Acad. Sci. USA* **118**, e2103518118 (2021).
16. Feringa, B. L. The art of building small: from molecular switches to molecular motors. *J. Org. Chem.* **72**, 6635–6652 (2007).

17. Meldal, M. & Tornøe, C. W. Cu-catalyzed azide-alkyne cycloaddition. *Chem. Rev.* **108**, 2952–3015 (2008).
18. Jensen, K. B. et al. New phenol esters for efficient pH-controlled amine acylation of peptides, proteins, and sepharose beads in aqueous media. *Bioconjug. Chem.* **33**, 172–179 (2022).
19. Tamara, S., den Boer, M. A. & Heck, A. J. R. High-resolution native mass spectrometry. *Chem. Rev.* **122**, 7269–7326 (2022).
20. Uchikawa, E., Choi, E., Shang, G., Yu, H. & Bai, X. C. Activation mechanism of the insulin receptor revealed by cryo-EM structure of the fully liganded receptor–ligand complex. *eLife* **8**, e48630 (2019).
21. Wagner, A., Diez, J., Schulze-Briese, C. & Schluckebier, G. Crystal structure of ultralente—a microcrystalline insulin suspension. *Proteins* **74**, 1018–1027 (2009).
22. Croll, T. I. et al. Higher-resolution structure of the human insulin receptor ectodomain: multi-modal inclusion of the insert domain. *Structure* **24**, 469–476 (2016).
23. Lawrence, M. C. Understanding insulin and its receptor from their three-dimensional structures. *Mol. Metab.* **52**, 101255 (2021).
24. Gutmann, T. et al. Cryo-EM structure of the complete and ligand-saturated insulin receptor ectodomain. *J. Cell Biol.* **219**, e201907210 (2020).
25. Kristensen, C., Andersen, A. S., Ostergaard, S., Hansen, P. H. & Brandt, J. Functional reconstitution of insulin receptor binding site from non-binding receptor fragments. *J. Biol. Chem.* **277**, 18340–18345 (2002).
26. Jonassen, I. et al. Design of the novel protraction mechanism of insulin degludec, an ultra-long-acting basal insulin. *Pharm. Res.* **29**, 2104–2114 (2012).
27. Moody, A. J., Stan, M. A., Stan, M. & Gliemann, J. A simple free fat cell bioassay for insulin. *Horm. Metab. Res.* **6**, 12–16 (1974).
28. Ono, K., Takigawa, S. & Yamada, K. L-Glucose: another path to cancer cells. *Cancers* **12**, 850 (2020).
29. Tromans, R. A., Samanta, S. K., Chapman, A. M. & Davis, A. P. Selective glucose sensing in complex media using a biomimetic receptor. *Chem. Sci.* **11**, 3223–3227 (2020).
30. Pedersen, K. M. et al. Optimization of pig models for translation of subcutaneous pharmacokinetics of therapeutic proteins: liraglutide, insulin aspart and insulin detemir. *Transl. Res.* **239**, 71–84 (2022).
31. Kurtzhals, P., Østergaard, S., Nishimura, E. & Kjeldsen, T. Derivatization with fatty acids in peptide and protein drug discovery. *Nat. Rev. Drug Discov.* **22**, 59–80 (2023).
32. Bergman, R. N. Toward physiological understanding of glucose tolerance. Minimal-model approach. *Diabetes* **38**, 1512–1527 (1989).

Publisher's note Springer Nature remains neutral with regard to jurisdictional claims in published maps and institutional affiliations.



Open Access This article is licensed under a Creative Commons Attribution-NonCommercial-NoDerivatives 4.0 International License, which permits any non-commercial use, sharing, distribution and reproduction in any medium or format, as long as you give appropriate credit to the original author(s) and the source, provide a link to the Creative Commons licence, and indicate if you modified the licensed material. You do not have permission under this licence to share adapted material derived from this article or parts of it. The images or other third party material in this article are included in the article's Creative Commons licence, unless indicated otherwise in a credit line to the material. If material is not included in the article's Creative Commons licence and your intended use is not permitted by statutory regulation or exceeds the permitted use, you will need to obtain permission directly from the copyright holder. To view a copy of this licence, visit <http://creativecommons.org/licenses/by-nc-nd/4.0/>.

© The Author(s) 2024

Methods

Synthesis of buildings blocks, insulin conjugate NNC2215 and control compound NNC2215a

Detailed synthesis of NNC2215 and the control compound NNC2215a is described in the Supplementary information and in Extended Data Figs. 7–9. In brief, desB30 human insulin was conjugated at B29 to *O*-succinimidyl-pentyn-1-oxycarbonyl at pH > 10, and at B1 to *O*-peracetyl-D-glucosyl- β -ethylenoxy-acetic acid using Br CF₃ sulfonate phenolic active ester at pH 7.5. The acetyl groups were removed by gentle saponification. The macrocycle reagent was made from 3-(3,5-dimethylphenyl)propanoic acid by benzylic bromination, azidation, reduction of COOH to alcohol, and the azides were reduced to the amines, which were Boc-protected. The propyl alcohol was activated as the mesylate and transformed to the propyl azide. The three Boc-amino groups were transformed to the isocyanates using triflic anhydride, and the macrocycle was closed by reaction of the isocyanates with the previously described trisamino half-macrocycle reagent⁴. The roof azide macrocycle was triazole-coupled under Cu(I) catalysis with the given B29-alkyne insulin to give NNC2215, which was purified using high-performance LC. Chemical characterization is shown in the Supplementary information and Supplementary Data.

Glucose affinity of the free macrocycle propyl azide by calorimetry

The concentration of the free macrocycle (Extended Data Fig. 8i) in the cell was 50 μ M. The concentration of glucose added in the syringe was 3 mM. The injection volume was 10 μ l. The stirring speed was 310 rpm; all in 10 mM phosphate buffer, pH 7.4 at 25 °C. The obtained K_a was 10,200 M⁻¹, and the K_d was 98 μ M. Data were acquired on the MicroCal VP-ITC microcalorimeter and processed using the MicroCal software (MicroCal VP-ITC Analysis Add-On Software Package 7.20 for ORIGIN 7.0).

Affinity of NNC2215 towards glucose by native MS

Glucose solutions (18.75 μ M, 37.5 μ M, 75 μ M, 150 μ M, 300 μ M, 625 μ M, 1.25 mM, 2.5 mM, 5 mM, 10 mM, 20 mM) in presence of NNC2215 (0.5 mg ml⁻¹) were prepared in 75 mM NH₄Ac, pH 7.4. The compounds were buffer-exchanged into 75 mM NH₄Ac, pH 7.4 by Amicon ultracentrifugal devices with 3,000 Da molecular weight cut-off filters. Direct infusion using a standard ESI probe was performed on a UPLC-ESI-MS Synapt G2-S (Waters) system with a UPLC flow-through needle. No column was used, and the system was configured to allow sample flow directly from the sample manager to the electrospray ionization probe. Positive ionization mode was used and the samples were sprayed using a flow of 30 μ l min⁻¹ and an injection volume of 20 μ l. The capillary voltage was 1.2 kV, and the source temperature was 85 °C, while the desolvation temperature was 80 °C. A Genedata workflow was used to quantify the ratio bound using the intensity (TIC) of the bound glucose complex versus the unbound form, that is, $M + 1$ glucose/($M + (M + 1)$ glucose)). The ratio bound (%) versus the glucose concentration (mM) was plotted using GraphPad Prism (GraphPad). The apparent glucose equilibrium K_d was determined from the binding curves by fitting the data with a one-site total-binding model.

3D modelling studies

The structural models of NNC2215 were built using Maestro (Schrödinger release 2020-3)³³. The macrocycle model was adapted from the models shown previously⁴ and connected to insulin at B29²⁶ with the corresponding linker. The glucoside was built modifying B1. For the open configuration, the modifications were applied to the receptor-bound insulin in PDB 6PXV (chain E²⁰), with a glucose molecule bound in the macrocycle as in the previous model⁴. For the closed conformation, insulin from PDB 2VJZ (ref. 21) was modified, building the glucoside bound in the macrocycle based on the same macrocycle-glucose complex

model described above. Both models underwent further refinement and energy-minimization steps within Maestro. For the obtained closed state, we additionally ran a molecular dynamics simulation in explicit solvent to test the stability of the conformation. The OPLS3e force-field was used for models of NNC2215 bound to glucose, which were solvated water molecules based on simple point charge (SPC) model in sodium-neutralized simulation boxes. A real-space cut-off of 9 Å for Coulombic interactions was used throughout. Standard Desmond preparation and relaxation protocols were used³³, gradually warming up the system and releasing restrained heavy atoms, consisting of initial 100 ps in NVT ensemble with Brownian dynamics at 10 K with a 1 fs timestep and 12 ps in Langevin dynamics with a Berendsen thermostat, followed by two subsequent equilibration runs of 12 ps in NPT ensemble at 1 atm with a Berendsen barostat first at 10 K and then at 300 K, and finally 24 ps at 300 K in the same NPT ensemble with full release of heavy atom restraints. The final molecular dynamics production run consisted of 100 ns in NPT at 1 atm and 300 K, using the Martina-Tobias-Klein method. The final coordinates of both open and closed models were superimposed onto the bound insulin in PDB 6PXV (chain E) to show how the closed conformation would hinder the interaction with the insulin receptor. Figure 1b was generated using ChimeraX³⁴.

In vitro biology

hIR-A and IGF-1R affinity measurements. The following materials were used: SPA PVT antibody-binding beads, anti-mouse reagent (GE Healthcare, RPNQ0017), HSA (Sigma-Aldrich, A1887, SLCBR2530) and antibodies hIR 83.7 and IGF-1R 24-31 (produced at Novo Nordisk, licensed from K. Siddle^{35,36}).

BHK cells overexpressing hIR-A or IGF-1R were lysed in 50 mM HEPES pH 8.0, 150 mM NaCl, 1% Triton X-100, 2 mM EDTA and 10% glycerol. The cleared cell lysate was batch absorbed with WGA-agarose (Lectin from *Triticum vulgare*-Agarose, L1394, Sigma-Aldrich) for 90 min. The receptors were washed with 20 volumes 50 mM HEPES pH 8.0, 150 mM NaCl and 0.1% Triton X-100, after which the receptors were eluted with 50 mM HEPES pH 8.0, 150 mM NaCl, 0.1% Triton X-100, 0.5 M *n*-acetyl glucosamine and 10% glycerol³⁷. All buffers contained cOmplete protease inhibitor mixture (Roche Diagnostic).

Binding studies were performed with dilution series of ligands in 100 mM HEPES, 100 mM NaCl, 10 mM MgSO₄ and 0.025% (v/v) Tween-20, pH 7.4, with or without 1.5% HSA in the presence of 0, 3, 5, 10 or 20 mM D-glucose in triplicates for each dilution in 96-well Isoplates (PerkinElmer, 6005049), 5,000 CPM Tyr A14-¹²⁵I-insulin, 25 μ l SPA beads, 25 ng IR 83-7 antibody, 0.006 μ l hIR-A per well. After 22 h incubation at 22 °C, the bound radioactivity was quantified by counting in a Microbeta2 2450 Microplate counter (Perkin Elmer), essentially as described previously³⁷.

IGF-1R-binding assays were conducted essentially as for the IR binding assays, except that solubilized IGF-1Rs, [¹²⁵I-Tyr31]-human IGF-1 and the IGF-1R-specific antibody 24-31 were used as previously described³⁸.

The IC₅₀ and relative affinities to human insulin were calculated. Each point in the competition curve was a measure of triplicates with the mean and s.d. The IC₅₀ of the one-site binding model was fitted with a nonlinear regression algorithm using GraphPad Prism. The top, bottom and slope were set to be equal for all of the compounds in each experiment. As the logarithm cannot be calculated for zero, the concentration without unlabelled ligand was set to 1×10^{-14} M in the calculations. On each plate, human insulin was included for calculation of the relative affinities of NNC2215 and insulin degludec for each set of plates. The average and s.d. for three independent experiments were calculated using Excel. The fold changes in the relative affinity to hIR-A were calculated from 0 or 3 mM glucose to 20 mM glucose in each experiment and the average and s.d. were calculated.

hIR phosphorylation and AKT and ERK assays. In three independent experiments, CHO-hIR cells³⁹ were stimulated with increasing

Article

concentrations of human insulin and NNC2215 (0.1 μM) for 10 min. After stimulation, cells were homogenized in lysis buffer. Insulin receptor phosphorylation was measured in technical duplicate with the InsR(pY1158) Thermo Fisher Scientific ELISA kit according to the manufacturer's instructions. Phosphorylation of AKT and ERK were measured in technical duplicate using AlphaScreen, SureFire AKT1/2/3 (p-Ser473) and SureFire ERK1/2 p-T202/Y204 Assay Kits from PerkinElmer according to the manufacturer's instructions and a previous study³⁹.

Lipogenesis in primary mouse adipocytes. In primary rat mouse adipocytes isolated from epididymal fat pads, the effect of NNC2215 and insulin degludec on lipogenesis was determined by measuring the incorporation of [³H]-labelled glucose into fat as described previously²⁷ with a slight modification: L-glucose was added to a final concentration of 3 mM or 20 mM.

In vivo studies

Animal experiments were performed under a license granted by the Danish national Animal Experiments Inspectorate and complied with relevant ethical regulations on animal research.

L-Glucose rat model. Non-fasted healthy male Sprague–Dawley rats (aged 11 weeks; 380–430 g) were dosed i.v. with NNC2215 or insulin degludec (4.5 nmol kg^{-1}) at timepoint zero. Then, 30 min later, the rats received an additional i.v. dosing of vehicle or 0.5, 1 or 2 g kg^{-1} L-glucose ($n = 7$ per group). Blood was drawn from the sublingual vein into EDTA Eppendorf tubes at timepoints 0, 25, 35, 45, 60, 90 and 120 min and immediately centrifuged for quantification of plasma D-glucose concentrations by the glucose oxidase technique (Biosen, EKF Diagnostics) and NNC2215 or insulin degludec plasma concentrations. The rats had no access to food during the experiment.

Hypoglycaemia study in pigs. Female LYD pigs aged approximately 18 weeks and weighing between 74.5 and 86.5 kg on the day of the first dose were used. Body weight increased to 99–110 kg on the day of the last dose. Before the experiments, all of the animals were instrumented with two venous catheters, one for infusion and one for sampling. Fasting glucose was measured before each experimental day and ranged from 4.43 to 6.23 mM. Animals were subjected to constant i.v. infusions of somatostatin (1 $\mu\text{g kg}^{-1} \text{min}^{-1}$)—to suppress endogenous insulin and glucagon secretion—and glucagon (0.45 $\text{pmol kg}^{-1} \text{min}^{-1}$) to replace the suppressed glucagon secretion. Suppression of insulin secretion was verified by measuring C-peptide levels, which documented that endogenous insulin secretion was below basal levels throughout the experiment despite plasma glucose being elevated (Extended Data Fig. 3c). Primed constant infusions of NNC2215 or insulin degludec and infusion of glucose were given as indicated below. Suitable priming doses of each insulin analogue were estimated based on their pharmacokinetics after i.v. administration.

The duration of the experiment was 540 min. At time 0, infusions of hormones and glucose were started. Glucose was infused at 6 $\text{mg kg}^{-1} \text{min}^{-1}$ from 0 to 360 min after which it was turned off for 90 min and restarted at 6 $\text{mg kg}^{-1} \text{min}^{-1}$ for the last 90 min of the experiment. To investigate a range of plasma glucose concentrations before turning off the glucose infusion, different insulin infusion rates were used (NNC2215: 1.30, 1.44, 1.58, 1.72, 1.86, 2.00 and 2.14 $\text{pmol kg}^{-1} \text{min}^{-1}$; insulin degludec: 0.7, 0.9 and 1.1 $\text{pmol kg}^{-1} \text{min}^{-1}$). The insulin infusion rates were chosen with the aim of having comparable glucose concentrations for NNC2215 and insulin degludec before turning off the glucose infusion. Owing to the limited experience with the glucodynamic potency of NNC2215, a broader dose range was tested for NNC2215 than for insulin degludec. The lower infusion rates of NNC2215 were tested at the beginning of the study and the higher rates were tested at the end of the study. Samples for glucose determination were drawn into EDTA Eppendorf tubes. The samples were then immediately centrifuged,

and the plasma analysed using the glucose oxidase technique (YSI 2900, YSI).

s.c. and i.v. pharmacokinetic study of NNC2215 in pigs. Seven female LYD pigs aged approximately 22 weeks and weighing between 93.0 and 97.5 kg were used. Before the experiment, the animals were instrumented with a venous catheter for i.v. injection of NNC2215 and for blood sampling. Four animals were injected s.c. in the neck area with 2 nmol kg^{-1} NNC2215 (600 nmol ml^{-1}) and three animals received i.v. bolus administration of 0.3 nmol kg^{-1} NNC2215. Blood samples were drawn into EDTA Eppendorf tubes and immediately centrifuged for quantification of plasma glucose concentrations by the glucose oxidase technique (Biosen; EKF Diagnostics) and NNC2215 plasma concentrations.

Pharmacokinetic/pharmacodynamic models. Methodology on the pharmacokinetic/pharmacodynamic modelling used to quantify the change in insulin activity of NNC2215 with changing plasma glucose based on data from the hypoglycaemia study in pigs is provided in the Supplementary information.

Glucose challenge study in diabetic rats. Healthy male Sprague–Dawley rats (aged approximately 9–10 weeks; 350–400 g) were surgically instrumented with permanent arterial (blood sampling) and venous (insulin and glucose infusions) catheters under isoflurane anaesthesia and recovered from surgery with analgesia (carprofen, 5 mg per rat per day, s.c.) for 7–8 days before being made acutely diabetic with streptozotocin (65 mg kg^{-1} , s.c.). Then, 3–4 days after streptozotocin treatment, the rats were fasted overnight and subjected to one of three different constant i.v. infusion rates of either NNC2215 (42, 84, 100 $\text{pmol kg}^{-1} \text{min}^{-1}$; primed, see below) or human insulin (20, 25, 30 $\text{pmol kg}^{-1} \text{min}^{-1}$) to lower plasma glucose from ≥ 15 mM to a predefined target of 5.7 mM. Appropriate priming doses of NNC2215 to obtain steady state in plasma exposure within the duration of the study was calculated using its pharmacokinetics after i.v. administration in rats. When the glucose target was reached, it was clamped by adjusting the i.v. GIR. When the GIR had been at steady state for at least 30 min, a GTT was carried out by infusing an additional 25 $\text{mg kg}^{-1} \text{min}^{-1}$ of glucose for 60 min on top of the individual steady-state GIR without clamping the plasma glucose. Blood for measurement of plasma glucose concentrations was drawn from the arterial catheter into heparinized Eppendorf tubes and immediately centrifuged for 30 s. Plasma glucose was measured every 10 min throughout the study by the glucose oxidase technique (YSI 2900). To mimic the effect of a glucose-sensitive insulin and to quantify its extra effect during the GTT, another group of streptozotocin diabetic rats was given 50% additional human insulin on top of the constant human insulin infusion (20 + 10 $\text{pmol kg}^{-1} \text{min}^{-1}$; human insulin +50%) during the GTT. The maximal plasma glucose concentrations during the GTT were compared using one-way analysis of variance and pairwise comparisons by Tukey's post hoc test.

Quantification of insulin and C-peptide concentrations in plasma samples. The plasma samples were analysed for levels of NNC2215, insulin degludec and human insulin using luminescence oxygen channeling immunoassay (LOCI)/Alpha-LISA, which is a homogeneous immunoassay method without washing steps. In the LOCI/Alpha-LISA assay, streptavidin-coated donor beads are used (Alpha-LISA donor beads, Perkin Elmer) in addition to acceptor beads (Alpha-LISA acceptor beads, Perkin Elmer), which were conjugated to a monoclonal antibody specific for the insulin analogues of interest (NNC2215, insulin degludec or human insulin). A second monoclonal antibody recognizing another part of the insulin analogues of interest was biotinylated and used in the LOCI/Alpha-LISA assay. The antibody pairs used for determination of the three analytes were as follows: NNC2215 (monoclonal antibody HUI-018 conjugated to acceptor beads and biotinylated polyclonal antibody GP

a-HI 4080-E; when measuring NNC2215 in pig plasma, unmarked monoclonal antibody OXI-005 was added to prevent measurement of endogenous pig insulin; when measuring in rat plasma, unmarked monoclonal antibodies anti-rat insulin 1 and anti-rat insulin 2 were added to prevent measurement of endogenous rat insulin); insulin degludec (monoclonal antibody NN454-1F31 conjugated to acceptor beads and biotinylated monoclonal antibody S1); human insulin in rat plasma (monoclonal antibody HUI-018 conjugated to acceptor beads and biotinylated monoclonal antibody OXI-005). All of the indicated antibodies were generated in-house at Novo Nordisk. A dilution row of NNC2215, insulin degludec or human insulin was prepared as calibrators in species-specific plasma pools in appropriate concentration ranges. The calibrator curves for each of the insulin analogues were used for the quantification of the specific analytes in unknown samples. Plasma samples containing the analytes of interest were incubated with antibody-coated acceptor beads in addition to the described biotinylated monoclonal antibody (Bio-mAb) in 384-well plates. After 1 h (insulin degludec and human insulin) or 24 h (NNC2215) of incubation, the streptavidin-coated donor beads were added to the wells. The acceptor beads, the analyte of interest, the Bio-mAb and the donor beads all form a complex within the solution. Illumination of the complex releases singlet oxygen atoms from the donor beads. These are channelled into the acceptor beads and trigger a chemiluminescence response, which is measured in an Envision plate reader (Perkin Elmer). The amount of light is proportional to the concentration of the analyte. The lower limit of quantification was determined to be 42 pM in LYD pig and 27 pM in rat for NNC2215, 15 pM in LYD pig for insulin degludec and 2.6 pM in rat for human insulin.

Plasma samples were analysed for pig C-peptide content using LOCI/AlphaLISA technology as described above for quantification of insulin concentrations in plasma samples. During the assay, a concentration-dependent bead-analyte-immune complex is created, resulting in light output, which is measured on the Perkin Elmer Envision reader. In the assay, anti-pig C-peptide monoclonal antibody M-grC-pe-1F34A1-conjugated acceptor beads and biotinylated monoclonal antibody 4F16A6 (also raised against pig C-peptide) were used together with generic streptavidin-coated donor beads. Both antibodies were made in house. The lower limit of quantification was 45 pM.

Reporting summary

Further information on research design is available in the Nature Portfolio Reporting Summary linked to this article.

Data availability

Source files of the 3D structural models of NNC2215 shown in Fig. 1b are available at Figshare (<https://doi.org/10.6084/m9.figshare.26526460>).

All other data supporting the findings of this study are available within the Article and its Supplementary information and Supplementary Data. Source data are provided with this paper.

33. Shaw Research. Desmond Molecular Dynamics System release 2020-3 (Schrödinger, 2020).
34. Pettersen, E. F. et al. UCSF ChimeraX: structure visualization for researchers, educators, and developers. *Protein Sci.* **30**, 70–82 (2021).
35. Soos, M. A. et al. Monoclonal antibodies reacting with multiple epitopes on the human insulin receptor. *Biochem. J.* **235**, 199–208 (1986).
36. Soos, M. A. et al. A panel of monoclonal antibodies for the type I insulin-like growth factor receptor. Epitope mapping, effects on ligand binding, and biological activity. *J. Biol. Chem.* **267**, 12955–12963 (1992).
37. Andersen, M., Nørgaard-Pedersen, D., Brandt, J., Pettersson, I. & Slaaby, R. IGF1 and IGF2 specificities to the two insulin receptor isoforms are determined by insulin receptor amino acid 718. *PLoS ONE* **12**, e0178885 (2017).
38. Hansen, B. F. et al. Molecular characterisation of long-acting insulin analogues in comparison with human insulin, IGF-1 and insulin X10. *PLoS ONE* **7**, e34274 (2012).
39. Hansen, B. F. et al. Sustained signalling from the insulin receptor after stimulation with insulin analogues exhibiting increased mitogenic potency. *Biochem. J.* **315**, 271–279 (1996).
40. Hoeg-Jensen, T. et al. Glucose sensitive insulins and uses thereof. Patent WO/2020/058322 (2020).

Acknowledgements We thank K. Holmberg, A. Hansen, R. J. Andersen, H. Jensen, H. Gudmundsdottir, C. S. Stenvang, C. Dengsøe, M. Okkels, B. Kolling, G.-M. Nelander, P. Jensen, J. Damgaard, L. Hansen, B. Hansen, B. L. Bengtsen, S. L. Riisberg, M. Hvidt, W. Liu, T. Østergaard, K. B. Jensen, L. Christiansen, S. Jørgensen and animal caretakers for expert technical assistance; J. Cvačka and E. Kofroňová for small-molecule HR-ESI-MS measurements; and C. Roepstorff for providing medical writing support funded by Novo Nordisk. This study was funded by Novo Nordisk.

Author contributions T.H.-J., T.K., A.R.M., L.L., K.S.H. and P.S. designed and prepared the insulin conjugates. T.H.-J., T.K., P.S., A.P.D., R.A.T., M.T., G.P.-H., D.J.L., M.G.O. and A.C. designed and prepared the macrocycle building blocks. T.H.-J., L.L., P.S., S.K. and V.K. designed and prepared the glucoside building block. P.K.N. and G.I. did the biophysical characterizations. D.G. and E.J. performed structural modelling. R.S., B.F.H., T.A.P. and E.N. designed and performed the in vitro biology studies. C.L.B., J.S., C.F., K.-M.P., H.H.F.R., L.A., J.K., J.J.F. and A.V.N.-W. designed and performed the in vivo studies and analysis. T.H.-J. wrote the manuscript with assistance from all of the other authors.

Competing interests T.H.-J., T.K., C.L.B., J.S., C.F., P.K.N., E.N., A.R.M., L.L., K.S.H., G.I., E.J., D.G., B.F.H., T.A.P., J.K., K.-M.P., H.H.F.R., L.A., J.J.F., A.V.N.-W., P.S. and R.S. are current or previous employees and shareholders of Novo Nordisk. A.P.D., R.A.T., M.T., M.G.O. and A.C. are listed as inventors on patent WO2018167503 (Davis, A. et al., macrocyclic compounds, 20 September 2018). T.H.-J., T.K., A.R.M., A.P.D., A.C. and P.S. are listed as inventors on patent WO2020058322 (Hoeg-Jensen, T. et al., glucose sensitive insulins and uses thereof, 26 March 2020). T.H.-J., T.K., A.R.M., L.L., K.S.H., A.P.D., M.T., A.C., P.S. and R.S. are listed as inventors on patent WO202314240 (Hoeg-Jensen, T. et al., glucose sensitive insulin derivatives and uses thereof, 3 August 2023). The other authors declare no competing interests.

Additional information

Supplementary information The online version contains supplementary material available at <https://doi.org/10.1038/s41586-024-08042-3>.

Correspondence and requests for materials should be addressed to Rita Slaaby.

Peer review information Nature thanks David Sacks and the other, anonymous, reviewer(s) for their contribution to the peer review of this work. Peer reviewer reports are available.

Reprints and permissions information is available at <http://www.nature.com/reprints>.

Article

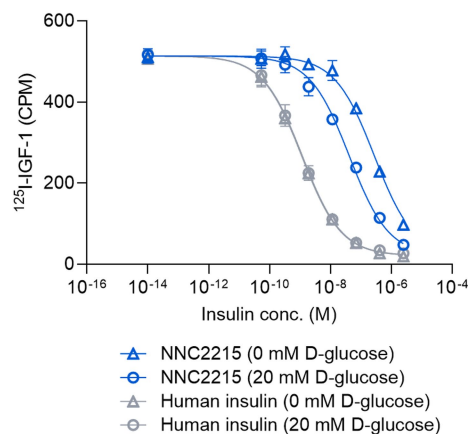
a IR affinity of NNC2215 (no HSA)

	hIR-A affinity relative to human insulin ^a (%)		Fold change 0 to 20 mM D-glucose
	D-glucose (mM)		
	0	20	
NNC2215	4.3 ± 0.9	28.3 ± 3.1	6.8 ± 1.7

b IR affinity of NNC2215a (1.5% HSA)

	hIR-A affinity relative to human insulin ^b (%)		Fold change 0 to 20 mM D-glucose
	D-glucose (mM)		
	0	20	
NNC2215a	5.8 ± 1.7	13.3 ± 1.7	2.4 ± 0.5

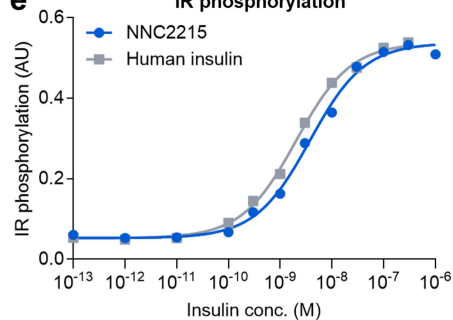
c IGF-1R binding



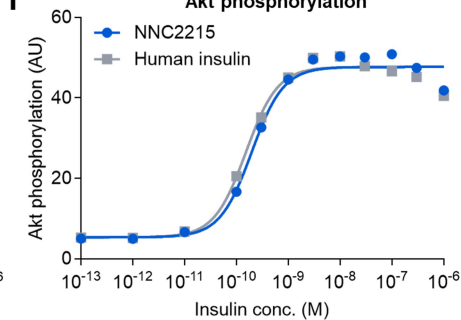
d IGF-1R affinity of NNC2215 (no HSA)

	hIGF-1R affinity relative to human insulin ^c (%)		Fold change 0 to 20 mM D-glucose
	D-glucose (mM)		
	0	20	
NNC2215	0.4 ± 0.03	2.9 ± 0.3	6.7 ± 0.5

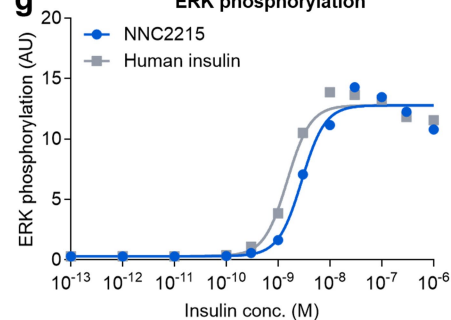
e IR phosphorylation



f Akt phosphorylation

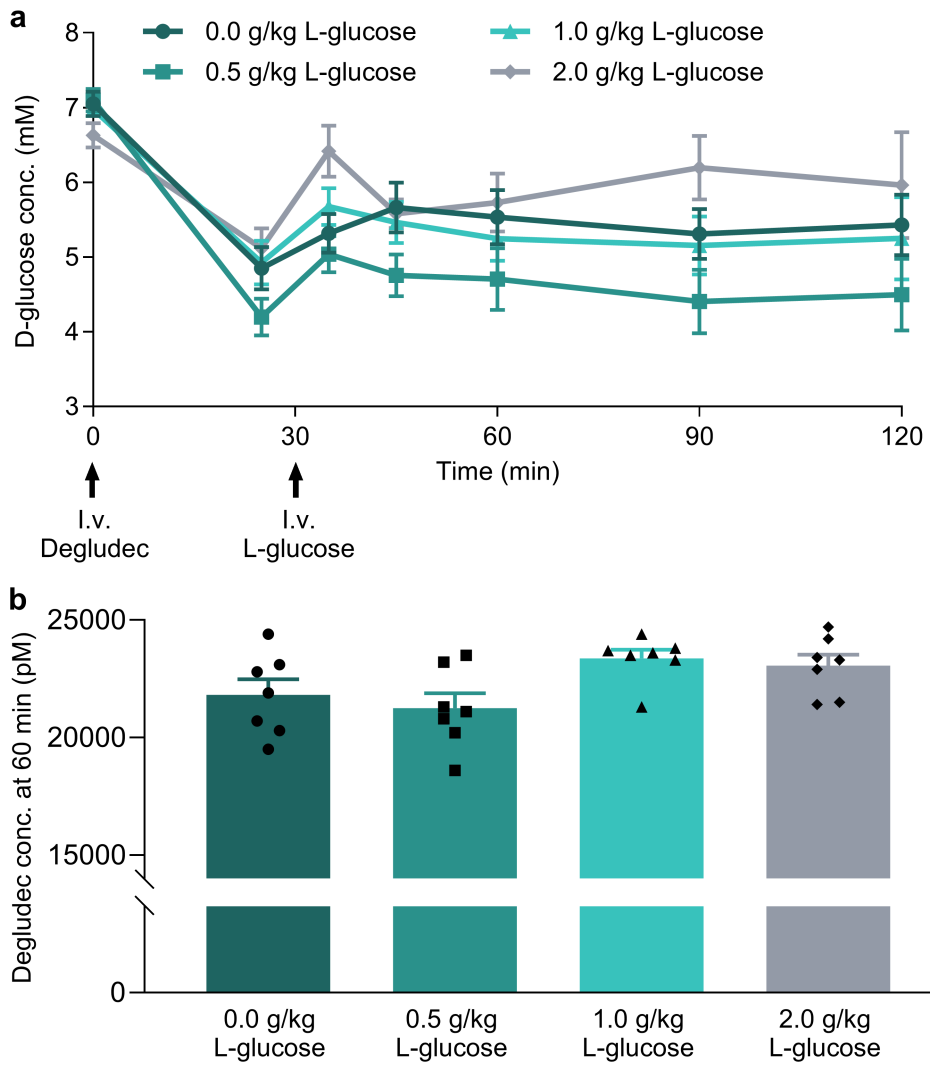


g ERK phosphorylation



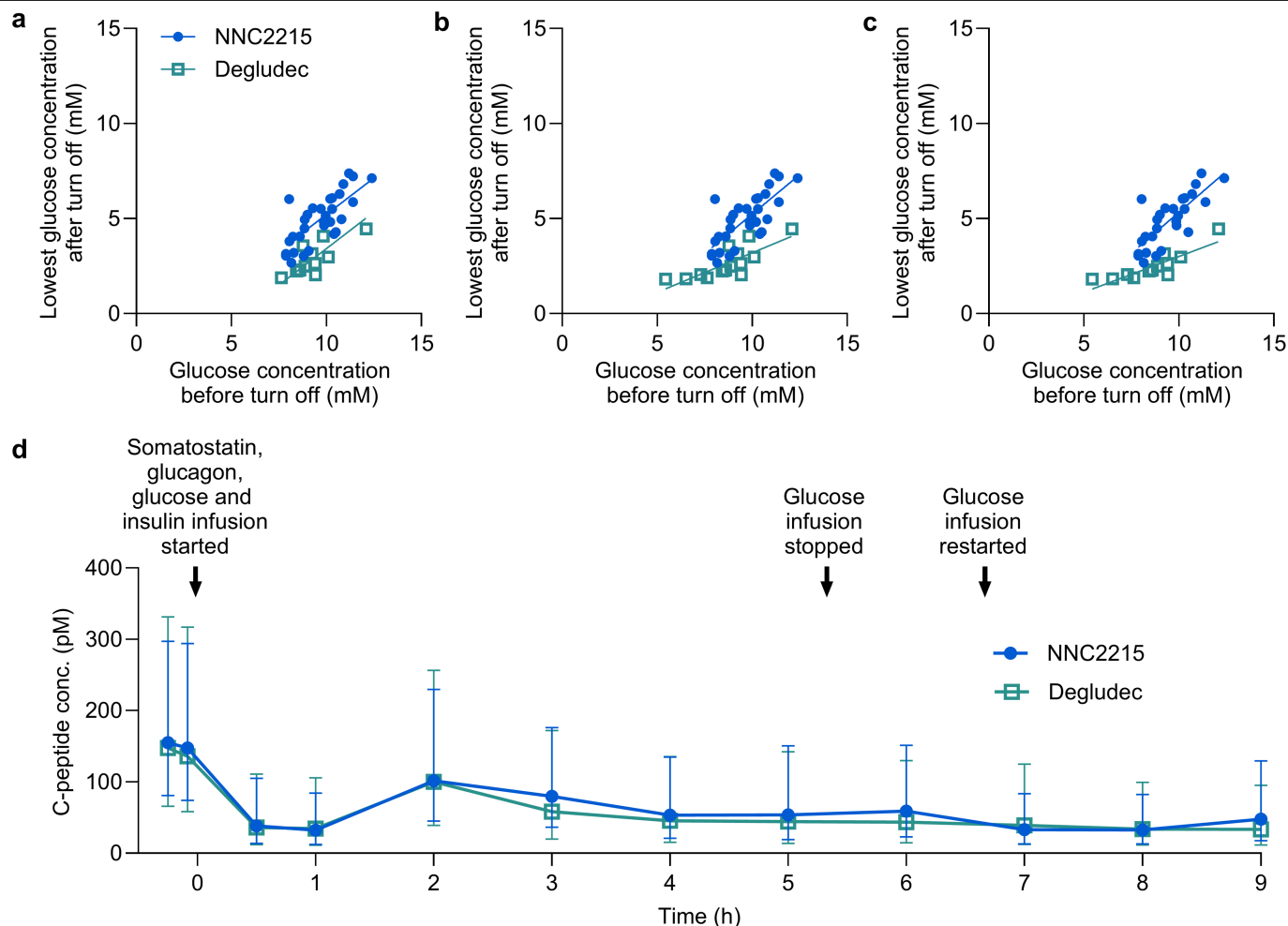
Extended Data Fig. 1 | In vitro biology. **a**, Glucose-dependent hIR-A affinity of NNC2215 with no HSA in the assay. Data are mean ± SD (n = 3 independent replicates). In each set of experiments the measurements were performed with three technical replicates. ^aDetermined from the IC₅₀ in the presence of 0 or 20 mM D-glucose (without HSA). **b**, Glucose-dependent hIR-A affinity of NNC2215a with 1.5% HSA in the assay. Data are mean ± SD (n = 3 independent replicates). In each set of experiments the measurements were performed with three technical replicates. ^bDetermined from the IC₅₀ in the presence of 0 or 20 mM D-glucose (with 1.5% HSA). **c**, Representative displacement curves of ¹²⁵I-IGF-1 from hIGF-1R for NNC2215 and human insulin in the presence of 0 or

20 mM D-glucose. Data are mean ± SD (n = 3 technical replicates). For some data points, the SD error bars are shorter than the size of the symbols. **d**, Glucose-dependent IGF-1R affinity of NNC2215 with no HSA in the assay. Data are mean ± SD (n = 3 independent replicates). In each set of experiments the measurements were performed with three technical replicates. ^dDetermined from the IC₅₀ in the presence of 0 or 20 mM D-glucose (without HSA). **e-g**, Representative curves of IR (**e**), Akt (**f**) and ERK (**g**) phosphorylation in CHO-hIR cells induced by increasing concentrations of NNC2215 or human insulin. Data are mean (n = 2 technical replicates).



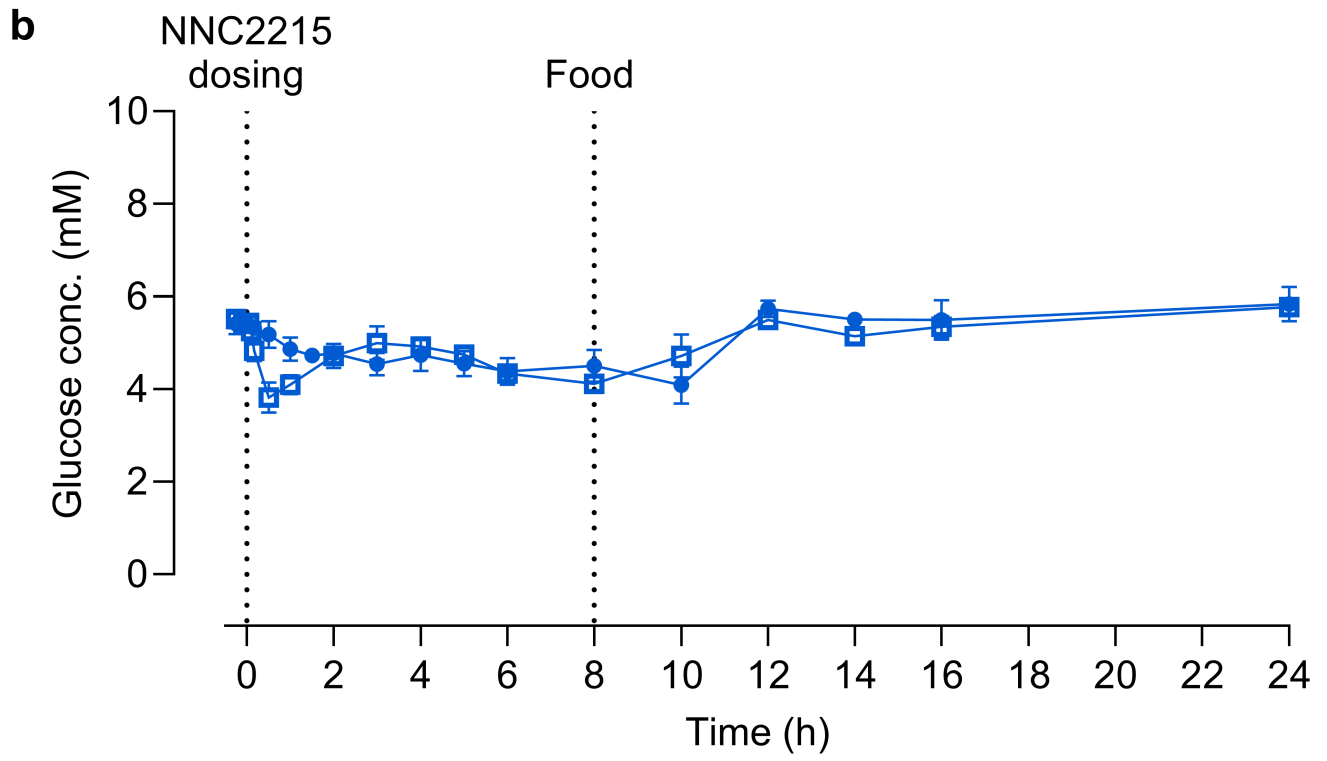
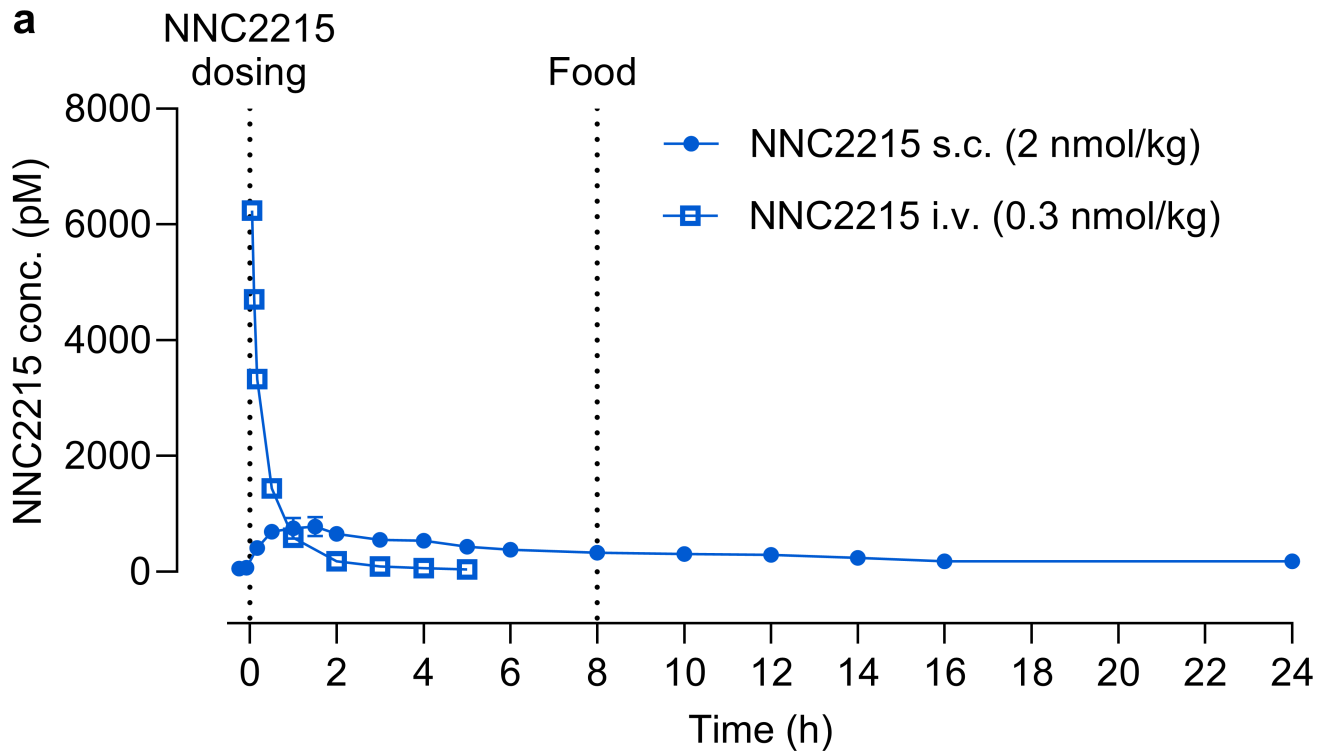
Extended Data Fig. 2 | L-glucose triggering experiment in vivo with the glucose non-sensitive insulin analogue, insulin degludec, as negative control. **a**, D-glucose levels did not decrease after dosing rats i.v. with increasing L-glucose doses (0 to 2 g/kg). Data are mean \pm SEM (n = 7 animals per group).

b, Glucose dose-independent clearance of insulin degludec measured by the insulin degludec concentration at 60 min. Data are mean \pm SEM (n = 7 animals per group).



Extended Data Fig. 3 | Hypoglycaemia study in pigs - Analysis of protection against hypoglycaemia and C-peptide concentrations. **a-c**, Exploratory correlation analyses of the lowest glucose concentration after turning off the glucose infusion vs. the glucose concentration immediately prior to turning off the glucose infusion. Nonlinear least squares regression analysis was performed using GraphPad Prism. All doses are contained in the plots. In (a) the insulin degludec data set has been truncated so the range of glucose concentrations before turning off glucose infusion is the same in the two groups. Slopes for NNC2215 and insulin degludec are not statistically significantly different ($p = 0.293$) as tested using an extra sum-of-squares F test. Intercepts for NNC2215 and insulin degludec are statistically significantly different ($p < 0.0001$) as tested using an extra sum-of-squares F test. The estimated difference in the drop in glucose between NNC2215 and insulin degludec was 1.8 mM. In (b) data from all pigs are shown, including those insulin degludec treated pigs with lower starting glucose values, illustrating that counterregulation sets in in

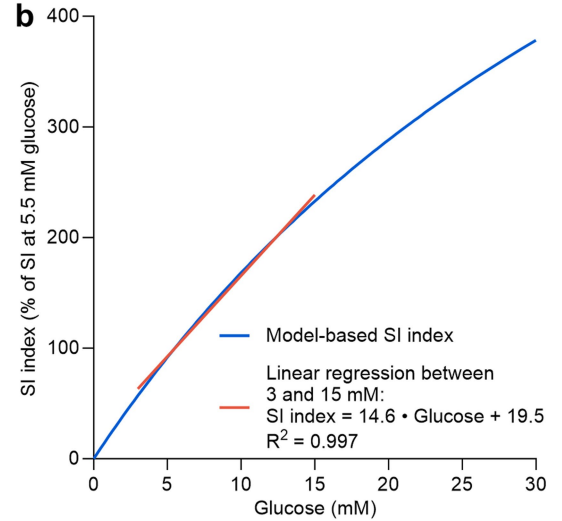
those pigs and the estimated slope becomes significantly different ($p = 0.024$) as tested using an extra sum-of-squares F test. In (c) six data sets corresponding to all six experimental days in a single animal with high C-peptide levels were omitted, which does not alter the conclusion that can be drawn from (b). **d**, C-peptide concentrations. Data are geometric mean ± geometric SD ($n = 31$ animals for NNC2215 and $n = 15$ animals for insulin degludec). Data are plotted across all dose levels documenting suppression of C-peptide despite relative hyperglycaemia in the pigs during the experiment. Suppression was not different in NNC2215 and insulin degludec treated pigs. During the experiment, most values were below the lower limit of quantification of 45 pM and those were represented as 22.5 pM. Occasional poor replicate C-peptide measurements were treated conservatively in relation to demonstrating C-peptide suppression by selection of the higher of the two replicates. Geometric mean was chosen due to one pig having markedly higher C-peptide levels than the rest, albeit still with lower values during infusion than at baseline.



Extended Data Fig. 4 | Pharmacokinetic profile and glucose concentration following s.c. and i.v. administration of NNC2215 in LYD pigs. a, NNC2215 concentrations in plasma. b, Plasma glucose levels. Data are mean \pm SEM (n = 4 animals for s.c. and n = 3 animals for i.v.).

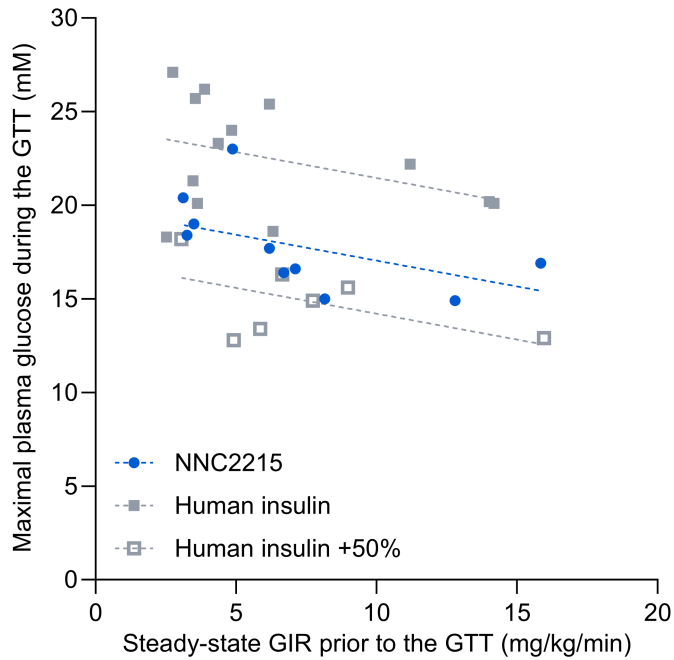
a

Parameter	Description	Unit	Parameter value
p2	Rate constant for loss of insulin action	1/h	0.372 ^a
SI _{max}	Maximum SI (insulin sensitivity)		0.00673
SI _{EC50}	Glucose level giving 50% of SI _{max}	mM	50 (fixed)
VG	Volume of distribution for glucose	l/kg	0.218 (fixed)
GB	Steady-state glucose level	mM	7.62 ^b
SG	Rate constant for insulin-independent glucose production and elimination	1/h	1.12
G0	Plasma glucose at time 0 (for initialisation)	mM	5.34
Residual error		%	10

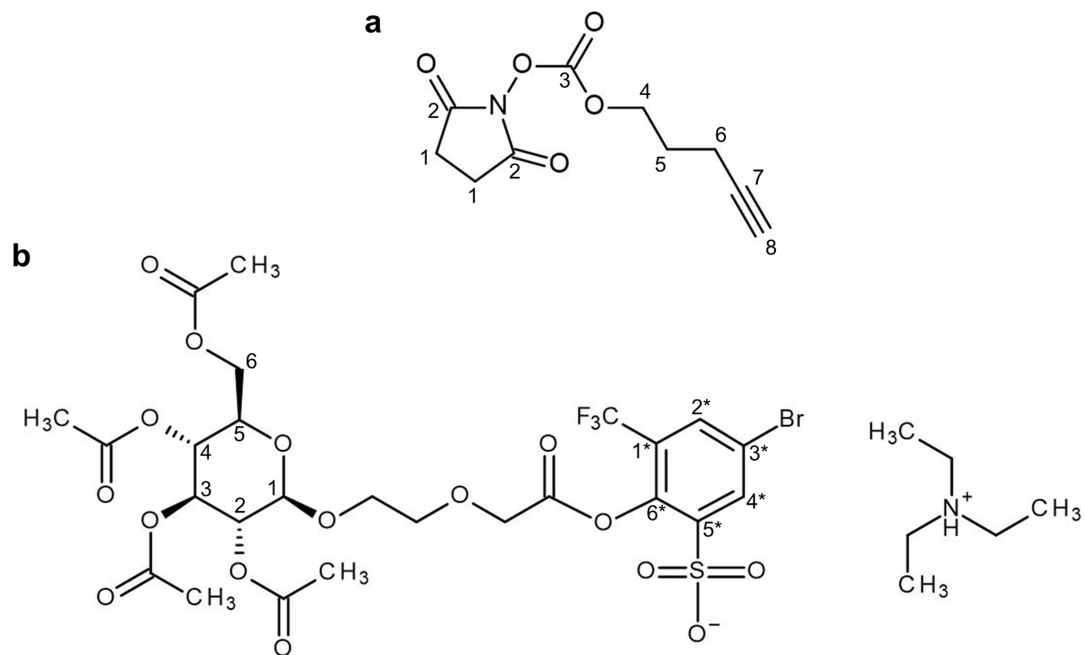


Extended Data Fig. 5 | Minimal model based on the hypoglycaemic study in LYD pigs quantifying the change in NNC2215 activity depending on glucose concentration. **a**, Parameters for the minimal model. Data are typical values from a non-linear mixed effects model. Endogenous insulin was confirmed by bioanalysis to have been suppressed by the somatostatin infusion, and hence this contribution was set to 0 in the model. ^aInterindividual variation: 86%.

^bInterindividual variation: 38%. Correlation with P2: 44%. **b**, Model-based SI index for NNC2215 as a function of plasma glucose. The simulation was based on typical values from the pharmacokinetic/pharmacodynamic model. SI was expressed as $0.00673 \cdot \text{Glucose concentration} / (50 + \text{Glucose concentration})$. The SI index for a given glucose concentration was calculated as the SI for that glucose concentration in percent of the SI for a glucose concentration of 5.5 mM.

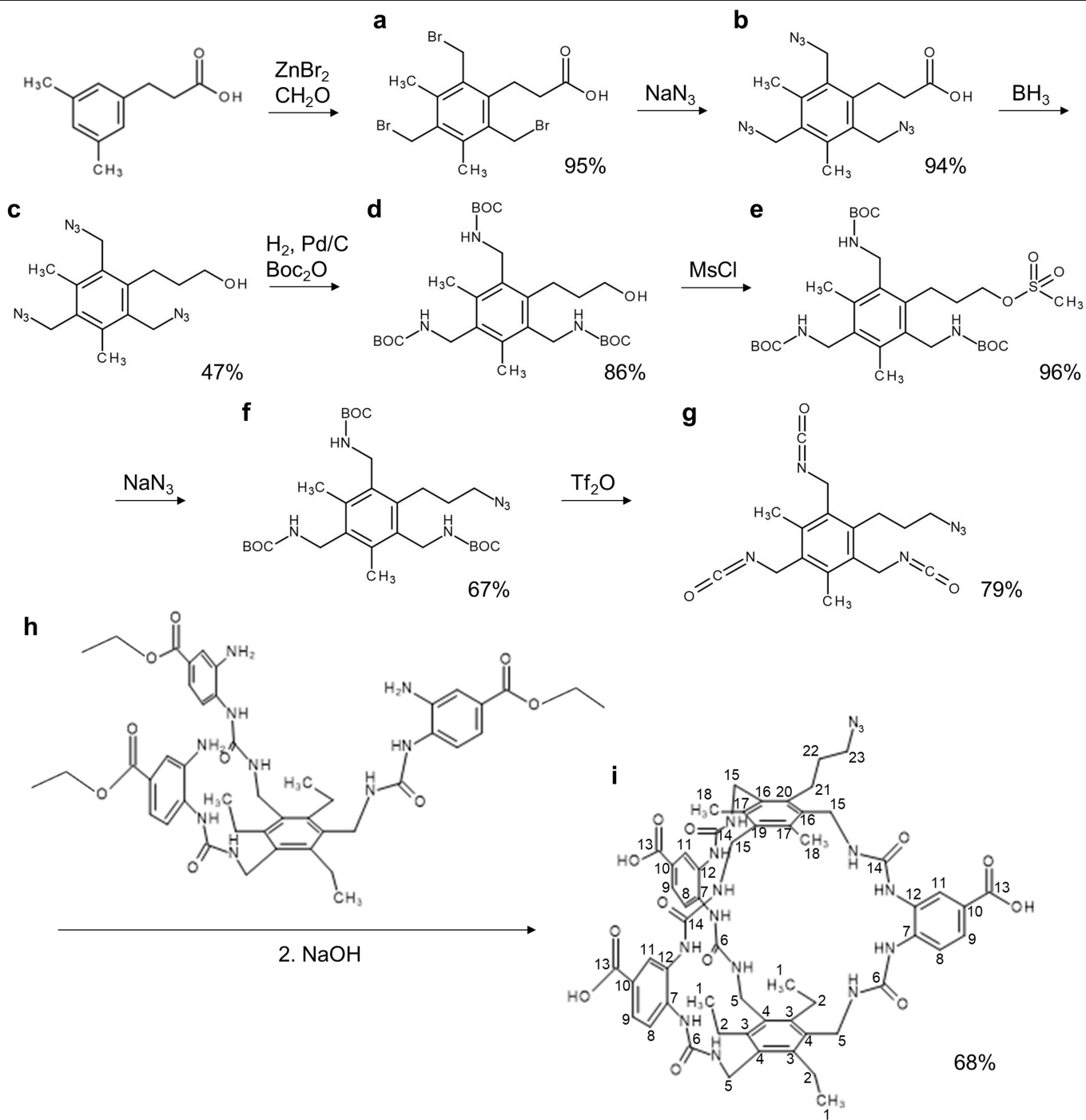


Extended Data Fig. 6 | Linear regression of maximal plasma glucose concentration during the GTT vs. steady-state GIR prior to the GTT in rats. For each animal, the maximal plasma glucose concentration during the GTT was plotted against the steady-state GIR prior to the GTT, which represents the quantitative effect of the constant insulin infusion. Nonlinear least squares regression analysis was performed using GraphPad Prism. Slopes for NNC2215, human insulin and human insulin +50% are not statistically significantly different ($p = 0.908$) as tested using an extra sum-of-squares F test. The slope for the three groups pooled is $-0.311 \text{ mM}/(\text{mg}/\text{kg}/\text{min})$. Importantly, the Y-axis intercepts (i.e. the maximal plasma glucose concentration during the GTT) for NNC2215, human insulin and human insulin +50% are statistically significantly different ($p < 0.0001$), as tested using an extra sum-of-squares F test, with the intercept of the NNC2215 group being in between the human insulin group, which was higher, and the human insulin +50% group, which was lower. Quantitatively, the maximal plasma glucose concentration during the GTT evaluated at $\text{GIR} = 0 \text{ mg}/\text{kg}/\text{min}$ prior to the GTT was reduced by 18% for NNC2215 vs. human insulin and by 30% for NNC2215 vs. human insulin +50%. Thus, the glucose sensitive effect of NNC2215 was less than the effect of 50% additional human insulin but corresponded more closely to 30% additional human insulin ($50\% \cdot 18/30$). Evaluated at $\text{GIR} = 15 \text{ mg}/\text{kg}/\text{min}$ prior to the GTT, the effect of NNC2215 during the GTT corresponded to 32% additional human insulin.



Extended Data Fig. 7 | *O*-succinimidyl pentyn-1-oxycarbonyl and beta-carboxymethyl-oxethyl-*O*-peracetyl-D-glucoside active ester. **a, *O*-succinimidyl pentyn-1-oxycarbonyl. **b**, beta-carboxymethyl-oxethyl-**

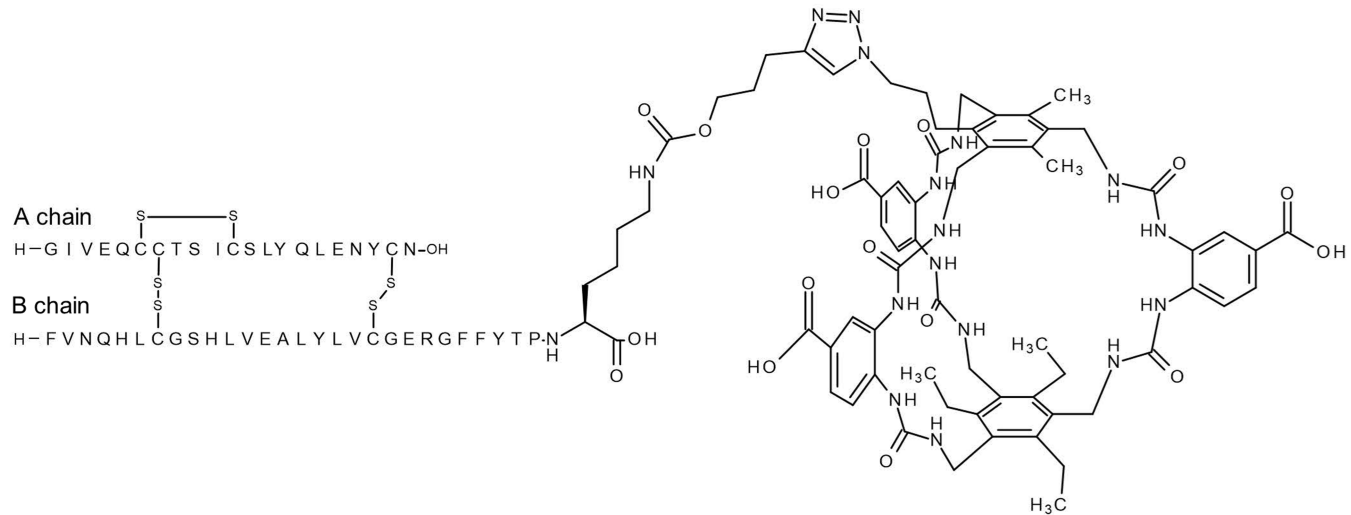
O-peracetyl-D-glucoside active ester. Carbon atoms are numbered to allow identification of the NMR assignments provided in the Supplementary Data.



Extended Data Fig. 8 | Synthesis of the macrocycle roof propyl azide.

a, Trisbromomethyl acid. **b**, Carboxy tris-azide. **c**, Alcohol tris-azide. **d**, Alcohol tris-Boc. **e**, *O*-mesylate tris-Boc. **f**, Azide tris-Boc. **g**, Propyl azide tris-isocyanate.

h, Compound 25c⁴⁰. **i**, Macrocycle roof propyl azide. Carbon atoms in (i) are numbered to allow identification of the NMR assignments provided in the Supplementary Data. Yields are given in percent.



Extended Data Fig. 9 | Control compound NNC2215a. The structure of the control compound NNC2215a.

Extended Data Table 1 | Non-compartmental and compartmental pharmacokinetic analysis

a

	Rat			LYD pig		
	Cl (L/h/kg)	V _z (L/kg)	T _½ (h)	Cl (L/h/kg)	V _z (L/kg)	T _½ (h)
NNC2215	0.20 ± 0.03	0.34 ± 0.06	1.19 ± 0.05	0.11 ± 0.01	0.20 ± 0.02	1.31 ± 0.02
Insulin degludec	0.04 ± 0.01	0.10 ± 0.04	1.65 ± 0.54	0.07 ± 0.01	0.19 ± 0.02	1.83 ± 0.08
Human insulin	5.26 ± 0.66	1.89 ± 0.32	0.25 ± 0.01	1.49 ± 0.48	0.28 ± 0.08	0.12 ± 0.04

b

Pharmacokinetic parameter	Unit	Parameter value
Volume of distribution of the central compartment	L/kg	0.0482
Volume of distribution of the peripheral compartment	L/kg	0.0723
Clearance	L/h/kg	0.131 ^a
Distribution clearance	L/h/kg	0.0621
Residual error	%	10.8

a, Non-compartmental analysis estimates of clearance, volume of distribution and elimination half-life of NNC2215, insulin degludec and human insulin after intravenous administration in rats and LYD pigs. Data are arithmetic mean ± SD for clearance and volume of distribution and harmonic mean ± pseudo SD for elimination half-life. Rat studies n=8 animals for NNC2215, n=5 animals for insulin degludec and n=3 animals for human insulin. LYD pig studies n=3 animals for NNC2215 and n=8 animals for insulin degludec and human insulin. **b**, Pharmacokinetic parameters for the 2-compartment model of NNC2215 in LYD pigs. Data are typical values from non-linear mixed effects model. ^aInterindividual variation: 34%.

Reporting Summary

Nature Portfolio wishes to improve the reproducibility of the work that we publish. This form provides structure for consistency and transparency in reporting. For further information on Nature Portfolio policies, see our [Editorial Policies](#) and the [Editorial Policy Checklist](#).

Statistics

For all statistical analyses, confirm that the following items are present in the figure legend, table legend, main text, or Methods section.

- | n/a | Confirmed |
|-------------------------------------|--|
| <input type="checkbox"/> | <input checked="" type="checkbox"/> The exact sample size (n) for each experimental group/condition, given as a discrete number and unit of measurement |
| <input type="checkbox"/> | <input checked="" type="checkbox"/> A statement on whether measurements were taken from distinct samples or whether the same sample was measured repeatedly |
| <input type="checkbox"/> | <input checked="" type="checkbox"/> The statistical test(s) used AND whether they are one- or two-sided
<i>Only common tests should be described solely by name; describe more complex techniques in the Methods section.</i> |
| <input type="checkbox"/> | <input checked="" type="checkbox"/> A description of all covariates tested |
| <input type="checkbox"/> | <input checked="" type="checkbox"/> A description of any assumptions or corrections, such as tests of normality and adjustment for multiple comparisons |
| <input type="checkbox"/> | <input checked="" type="checkbox"/> A full description of the statistical parameters including central tendency (e.g. means) or other basic estimates (e.g. regression coefficient) AND variation (e.g. standard deviation) or associated estimates of uncertainty (e.g. confidence intervals) |
| <input type="checkbox"/> | <input checked="" type="checkbox"/> For null hypothesis testing, the test statistic (e.g. F , t , r) with confidence intervals, effect sizes, degrees of freedom and P value noted
<i>Give P values as exact values whenever suitable.</i> |
| <input checked="" type="checkbox"/> | <input type="checkbox"/> For Bayesian analysis, information on the choice of priors and Markov chain Monte Carlo settings |
| <input checked="" type="checkbox"/> | <input type="checkbox"/> For hierarchical and complex designs, identification of the appropriate level for tests and full reporting of outcomes |
| <input checked="" type="checkbox"/> | <input type="checkbox"/> Estimates of effect sizes (e.g. Cohen's d , Pearson's r), indicating how they were calculated |

Our web collection on [statistics for biologists](#) contains articles on many of the points above.

Software and code

Policy information about [availability of computer code](#)

Data collection	MicroCal VP-ITC Analysis Add On Software Package 7.20 for ORIGIN 7.0 Maestro (Schrödinger release 2020 3) BIOVIA Discovery Studio (Version 4.0) BIOVIA Draw (Version 22.1)
Data analysis	Phoenix NLME (Version 8.4) GraphPad Prism (Version 10.2.1) Microsoft Excel for Microsoft 365 (Version 2406 Build 16.0.17726.20078)

For manuscripts utilizing custom algorithms or software that are central to the research but not yet described in published literature, software must be made available to editors and reviewers. We strongly encourage code deposition in a community repository (e.g. GitHub). See the Nature Portfolio [guidelines for submitting code & software](#) for further information.

Data

Policy information about [availability of data](#)

All manuscripts must include a [data availability statement](#). This statement should provide the following information, where applicable:

- Accession codes, unique identifiers, or web links for publicly available datasets
- A description of any restrictions on data availability
- For clinical datasets or third party data, please ensure that the statement adheres to our [policy](#)

Source files of the 3D structural models of NNC2215 shown in Figure 1b are available at <https://doi.org/10.6084/m9.figshare.26526460>. All other data that support the findings of this study are available within this paper, its Supplementary information and the Source data that are provided with this paper. Any additional information is available upon request.

Human research participants

Policy information about [studies involving human research participants and Sex and Gender in Research](#).

Reporting on sex and gender	<input type="text" value="No data from humans are included."/>
Population characteristics	<input type="text" value="No data from humans are included."/>
Recruitment	<input type="text" value="No data from humans are included."/>
Ethics oversight	<input type="text" value="No data from humans are included."/>

Note that full information on the approval of the study protocol must also be provided in the manuscript.

Field-specific reporting

Please select the one below that is the best fit for your research. If you are not sure, read the appropriate sections before making your selection.

- Life sciences Behavioural & social sciences Ecological, evolutionary & environmental sciences

For a reference copy of the document with all sections, see [nature.com/documents/nr-reporting-summary-flat.pdf](https://www.nature.com/documents/nr-reporting-summary-flat.pdf)

Life sciences study design

All studies must disclose on these points even when the disclosure is negative.

Sample size	<input type="text" value="No sample size calculations were performed. For the in vitro and ex vivo studies, the sample size was at least three biological replicates to be able to calculate a variability measure in addition to the mean. For the in vivo studies in rats and pigs, three to eight animals were included per group as typical for these types of studies."/>
Data exclusions	<input type="text" value="No data were excluded."/>
Replication	<input type="text" value="The native MS study included three technical replicates. The binding studies included three independent experiments and each independent experiment included two or three technical replicates. The cell based and in vivo studies included at least three biological replicates. Specific n values are provided in each table/figure legend. All attempts at replication were successful and all experimental data were reproducible between independent experiments."/>
Randomization	<input type="text" value="Randomization is not applicable for the included types of studies. For the in vivo studies in rats, animals were stratified into the required number of groups based on body weight."/>
Blinding	<input type="text" value="Blinding for experimental group allocation is not applicable for these types of studies. Firstly, to minimize the risk of making unintentional human errors during the experiments, the study protocols were kept as simple as possible, which included working with non-blinded study designs. Secondly, it is unlikely in these types of studies that the results can be affected by knowing the allocation to experimental groups."/>

Reporting for specific materials, systems and methods

We require information from authors about some types of materials, experimental systems and methods used in many studies. Here, indicate whether each material, system or method listed is relevant to your study. If you are not sure if a list item applies to your research, read the appropriate section before selecting a response.

Materials & experimental systems

n/a	<input type="checkbox"/>	Involvement in the study
<input type="checkbox"/>	<input checked="" type="checkbox"/>	Antibodies
<input type="checkbox"/>	<input checked="" type="checkbox"/>	Eukaryotic cell lines
<input checked="" type="checkbox"/>	<input type="checkbox"/>	Palaeontology and archaeology
<input type="checkbox"/>	<input checked="" type="checkbox"/>	Animals and other organisms
<input checked="" type="checkbox"/>	<input type="checkbox"/>	Clinical data
<input checked="" type="checkbox"/>	<input type="checkbox"/>	Dual use research of concern

Methods

n/a	<input type="checkbox"/>	Involvement in the study
<input checked="" type="checkbox"/>	<input type="checkbox"/>	ChIP-seq
<input checked="" type="checkbox"/>	<input type="checkbox"/>	Flow cytometry
<input checked="" type="checkbox"/>	<input type="checkbox"/>	MRI-based neuroimaging

Antibodies

Antibodies used	<p>Anti-hIR 83.7 (1212-0000-0228; Novo Nordisk; batch 4C), 25 ng per binding reaction</p> <p>Anti-IGF-1R 24-31 (1212-0000-0131; Novo Nordisk; batch 4B), 25 ng per binding reaction</p> <p>Quantification of NNC2215: Sandwich assay with combination of antibodies mAb HUI-018 (1212-0000-0087; Novo Nordisk; batch 27B; working concentration: 33.3 µg/mL acceptor beads conjugated with antibody) and biotinylated pAb GP a-HI 4080-E (Novo Nordisk; working concentration: 15 nM = 283x dilution).</p> <p>Quantification of insulin degludec: Combination of antibodies mAb NN454-1F31 (1212-0000-0096; Novo Nordisk; batch 17B; working concentration: 66.7 µg/mL acceptor beads conjugated with antibody) and biotinylated mAb S1 (1212-0000-0107; Novo Nordisk; batch 4B; working concentration: 3.27 nM).</p> <p>Quantification of human insulin: Combination of antibodies mAb HUI-018 (1212-0000-0087; Novo Nordisk; batch 27B; working concentration: 33.3 µg/mL acceptor beads conjugated with antibody) and biotinylated mAb OXI-005 (1212-0000-0415; Novo Nordisk; batch 3B; working concentration: 8 nM).</p> <p>Quantification of pig C-peptide: Combination of antibodies: mAb M-grC-pe-1F34A1 (1212-0000-0583; Novo Nordisk; batch 1B; working concentration: 33.3 µg/mL acceptor beads conjugated with antibody) and biotinylated mAb 4F16A6 (1212-000-0581; Novo Nordisk; batch 2B; working concentration: 12 nM).</p>
Validation	<p>Validation of the specificity of anti-hIR 83.7 for the insulin receptor and anti-IGF-1R 24-31 for the IGF-1R has previously been done by Soos, M. A. et al. (1986) <i>Biochem. J.</i> 235, 199-208 and Soos, M. A. et al. (1992) <i>J. Biol. Chem.</i> 267, 12955-12963. The specificity of the batches expressed in-house were qualified by immunoprecipitation and Western blot analysis.</p> <p>The antibodies for quantification of insulin, insulin analogues and C-peptide were produced at Novo Nordisk. Their identity and quality have been checked by using Nanodrop, SEC-HPLC, LC-MS and SDS Page. The combination of antibodies used in the assays were qualified for purpose by covering the following issues: 1) selectivity (cross reactivity of rat insulin in human insulin assay is <1% and cross reaction of pig insulin in C-peptide assay is <0.01%), 2) sensitivity and range, 3) inter- and intra-assay variability, 4) dilution linearity and 5) interference.</p>

Eukaryotic cell lines

Policy information about [cell lines and Sex and Gender in Research](#)

Cell line source(s)	Chinese Hamster Ovary cells (ATTC, Rockville, MD, USA) were transfected with cDNA encoding human insulin receptor (CHO-hIR) as described in Hansen et al. (1996) <i>Biochem J.</i> 315, 271-279.
Authentication	The CHO-hIR cells expressing the cloned human insulin receptor were not authenticated, but grew as expected with the appropriate selection pressure. The morphology was as expected, and it was confirmed that the cells expressed the insulin receptor.
Mycoplasma contamination	Negative for mycoplasma contamination.
Commonly misidentified lines (See ICLAC register)	No commonly misidentified cell lines were used in the study.

Animals and other research organisms

Policy information about [studies involving animals; ARRIVE guidelines](#) recommended for reporting animal research, and [Sex and Gender in Research](#)

Laboratory animals	<p>L-glucose rat model: Male Sprague-Dawley rats (11 weeks of age)</p> <p>Hypoglycaemia study in pigs: Female Landrace-Yorkshire-Duroc pigs (approximately 18 weeks of age)</p> <p>S.c. and i.v. pharmacokinetic study of NNC2215 in pigs: Female Landrace-Yorkshire-Duroc pigs (approximately 22 weeks of age)</p> <p>Glucose challenge study in diabetic rats: Male Sprague-Dawley rats (approximately 9-10 weeks of age)</p>
Wild animals	No wild animals were used
Reporting on sex	There is generally no need for sex segregation with insulin pharmacology
Field-collected samples	No field collected samples

Ethics oversight

Danish national Animal Experiments Inspectorate

Note that full information on the approval of the study protocol must also be provided in the manuscript.